Protofilaments, Filaments, Ribbons, and Fibrils from Peptidomimetic Self-Assembly: Implications for Amyloid Fibril Formation and Materials Science

Hilal A. Lashuel, Steven R. LaBrenz, Linda Woo, Louise C. Serpell,[‡] and Jeffery W. Kelly*

Contribution from the Department of Chemistry and The Skaggs Institute of Chemical Biology, The Scripps Research Institute, 10550 North Torrey Pines Road, MB12, La Jolla, California 92037, and Medical Research Council, Laboratory of Molecular Biology, Hills Road, Cambridge, CB2 2QH, United Kingdom

Received October 21, 1999

Abstract: Deciphering the mechanism(s) of β-sheet mediated self-assembly is essential for understanding amyloid fibril formation and for the fabrication of polypeptide materials. Herein, we report a simple peptidomimetic that self-assembles into polymorphic β-sheet quaternary structures including protofilaments, filaments, fibrils, and ribbons that are reminiscent of the highly ordered structures displayed by the amyloidogenic peptides Aβ, calcitonin, and amylin. The distribution of quaternary structures can be controlled by and in some cases specified by manipulating the pH, buffer composition, and the ionic strength. The ability to control β-sheet-mediated assembly takes advantage of quaternary structure dependent pK_a perturbations. Biophysical methods including analytical ultracentrifugation studies as well as far-UV circular dichroism and FT-IR spectroscopy demonstrate that linked secondary and quaternary structural changes mediate peptidomimetic self-assembly. Electron and atomic force microscopy reveal that peptidomimetic assembly involves numerous quaternary structural intermediates that appear to self-assemble in a convergent fashion affording quaternary structures of increasing complexity. The ability to control the assembly pathway(s) and the final quaternary structure(s) afforded should prove to be particularly useful in deciphering the quaternary structural requirements for amyloid fibril formation and for the construction of noncovalent macromolecular structures.

The self-assembly of peptides and proteins into noncovalent β-sheet rich quaternary structures, including fibrils, has attracted the attention of numerous laboratories owing to their association with neurodegenerative disease and their interesting structures.[1−10] In both amyloid and prion diseases a normally soluble protein or proteolytic fragment undergoes a conformational change either prior to, or coincident with, its self-assembly into β-sheet rich fibrils, implicated as the causative agent in numerous neurodegenerative diseases by genetic linkage.[11−19] Previous studies on amyloid fibril assembly establish the presence of quaternary structural intermediates, which appear to undergo convergent assembly into intermediates of increasing complexity until amyloid fibrils are ultimately afforded.[20−28] The differing quaternary structures observed could explain the strains char-

[‡] Laboratory of Molecular Biology.

(1) (a) Aggeli, A.; Bell, M.; Boden, N.; Keen, J. N.; Knowles, P. F.; Mcleish, T. C. B.; Pitkeathly, M.; Radford, S. E. *Nature* **1997**, *386*, 259−262. b) Aggeli, A.; Bell, M.; Boden, N.; Keen, J. N.; Mcleish, T. C. B.; Nyrkova, I.; Redford, S. E.; Semenov, A. *J. Mater. Chem.* **1997**, *7*, 1135−1145.

(2) Petka, W. A.; Hardin, J. L.; McGrath, K. P.; Wirtz, D.; Tirrell, D. A. *Science* **1998**, *281*, 389−392.

(3) Yamada, N.; Katsuhiko, A.; Naito, M.; Matsubara, K.; Koyama, E. *J. Am. Chem. Soc.* **1998**, *120*, 12192−12199.

(4) Janek, K.; Behlke, J.; Zipper, J.; Fabian, H.; Georgalis, Y.; Beyermann, M.; Bienert, M.; Krause, E. *Biochemistry* **1999**, *38*, 8246−8252.

(5) Shen, C. L.; Murphy, R. M. *Biophys. J.* **1995**, *69*, 640−651.

(6) Sorgehan, B.; Kosmoski, J.; Glabe, C. *J. Biol. Chem.* **1994**, *269*, 28551−28554.

(7) Koo, E. H.; Lansbury, P. T., Jr.; Kelly, J. W. *Proc. Natl. Acad. Sci. U.S.A.* **1999**, *96*, 9989−9990.

(8) Zhang, S.; Holmes, T.; Lockshin, C.; Rich, A. *Proc. Natl. Acad. Sci. U.S.A.* **1993**, *90*, 3334−3338.

(9) Burkoth, T. S.; Benzinger, T. L. S.; Jones, D. N. M.; Hallenga, K.; Meredith, S. C.; Lynn, D. G. *J. Am. Chem. Soc.* **1998**, *120*, 7655−7656.

(10) Benzinger, T. L.; Gregory, D. M.; Burkoth, T. S.; Miller-Auer, H.; Lynn, D. *Proc. Natl. Acad. Sci. U.S.A.* **1998**, *95*, 13407−13412.

(11) Selkoe, D. J. *J. Biol. Chem.* **1996**, *271*, 18295−18298.

(12) Selkoe, D. J. *Annu. Rev. Cell. Biol.* **1994**, *10*, 373−403.

(13) Hardy, J.; Allsop, D. *Trends Pharmacol. Sci.* **1991**, *12*, 383−388.

(14) Hardy, J. A.; Higgins, G. *Science* **1992**, *256*, 184−185.

(15) Jacobson, D. R.; Buxbaum, J. N. *Adv. Hum. Genet.* **1991**, *20*, 69−123.

(16) Jacobson, D. R.; Pastore, R. D.; Yaghoubian, R.; Kane, I.; Gallo, G.; Buck, F. S.; Buxbaum, J. N. *N. Engl. J. Med.* **1997**, *336*, 466−73.

(17) Howlett, D. R.; Jennings, K. H.; Lee, D. C.; Clark, M. S. G.; Brown, F.; Wetzel, R.; Wood, S. J.; Camilleri, P.; Roberts, G. W. *Neurodegeneration* **1995**, *4*, 23−32.

(18) Burdick, D.; Kosmoski, J.; Knauer, M. F.; Glabe, C. G. *Brain Res.* **1997**, *746*, 275−284.

(19) Pike, C. J.; Walencewicz-Wasserman, A. J.; Kosmoski, J.; Cribbs, H. D.; Glabe, C. G.; Cotman, C. W. *J. Neurochem.* **1995**, *64*, 253−265.

(20) Harper, J. D.; Wong, S. S.; Lieber, C. M.; Lansbury, P. T., Jr. *Chem. Biol.* **1997**, *4*, 119−125.

(21) Lashuel, H. A.; Lai, Z.; Kelly, J. W. *Biochemistry* **1998**, *37*, 17851−17864.

(22) Snyder, S. W.; Ladror, U. S.; Wade, W. S.; Wang, G. T.; Barrett, L. W.; Matayoshi, E. D.; Huffaker, H. J.; Krafft, G. A.; Holzman, T. F. *Biophys. J.* **1994**, *67*, 1216−1228.

(23) Giordano, T.; Pan, J. B.; Monteggia, L. M.; Holzman, T. F.; Snyder, S. W.; Kraft, G. A.; Ghanbari, H.; Kowall, N. W. *Exp. Neurol.* **1994**, *125*, 175−182.

(24) Kelly, J. W. *Curr. Opin. Struct. Biol.* **1998**, *8*, 101−106.

(25) Stine, W. B.; Snyder, S. W.; Ladror, U. S.; Wade, W. S.; Miller, M. F.; Perun, T. J.; Holzman, T. F.; Krafft, G. A. *J. Protein Chem.* **1996**, *15*, 193−203.

(26) Shen, C. L.; Fitzgerald, M. C.; Murphy, R. M. *Biophys. J.* **1995**, *67*, 1238−1246.

(27) Lomakin, A.; Chung, D. S.; Benedek, G. B.; Kirschner, D. A.; Teplow, D. B. *Proc. Natl. Acad. Sci. U.S.A.* **1996**, *93*, 1125−1129.

(28) Walsh, D. M.; Lomakin, A.; Benedek, G. B.; Condron, M. M.; Teplow, D. B. *J. Biol. Chem.* **1997**, *272*, 22364−22372.

10.1021/ja9937831 CCC: $19.00
Published on Web 05/19/2000

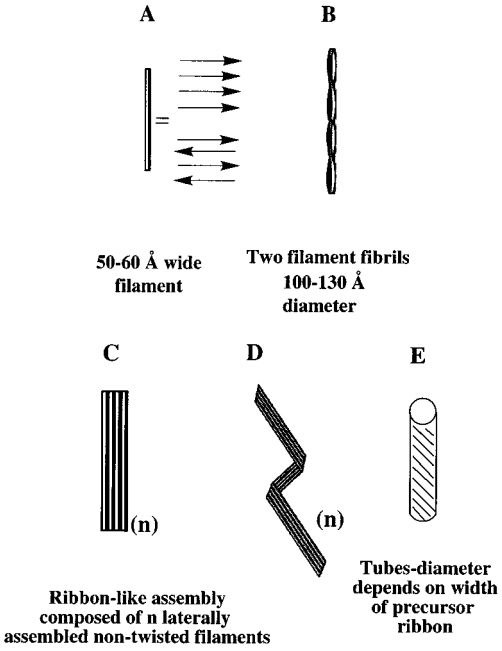

Figure 1. Schematic representation summarizing the quaternary structural species populated from the self-assembly of several amyloidogenic peptides and proteins illustrating: filaments (A), two-filament helical fibrils (B), ribbons (C), twisted ribbons (D), and tubes (E). The arrows (representing strands) next to the filament represents a cross-β structure (strands perpendicular to fibril axis) that can be parallel (top), antiparallel (bottom), or mixed (not shown). It is likely that filaments are composed of at least two sheets stacked face to face.

acterizing prion diseases and the variability in the neurotoxicity exhibited by different amyloid preparations.[17,29,30]

X-ray fibril diffraction data and electron microscopy observations on aggregates of several amyloidogenic proteins suggest a similar cross-β-sheet amyloid fibril structure, Figure 1A.[31−33] Amyloid fibrils appear to be composed of 2−6 filaments, each filament having a diameter of 50−60 Å, Figures 1A, B.[32,34−36] Several intermediates including filaments have been observed during the assembly of the Alzheimer's-associated Aβ peptides (1−40 or 1−42), implying that there are precursors to filaments which ultimately assemble into amyloid fibrils.[20,25,28,37−39] Numerous experimental studies suggest that filaments undergo further self-assembly to form amyloid fibrils with a helical twist (Figure 1B) and ribbon-like assemblies that are typically untwisted (Figure 1C), the latter are usually composed of > 3 filaments.[31,32,36,40−43] In the case of the amyloidogenic peptide calcitonin, these ribbon-like assemblies appear to twist back upon themselves (Figure 1D), ultimately affording hollow tube-like assemblies when the twist becomes severe enough that the edges of the twisted ribbons can interact (Figure 1E).[42] Easily synthesized peptidomimetics will be studied here to gain insight into the requirements for the formation of these quaternary structures.

Our laboratory has previously reported a cationic 2,8-dibenzofuran-bis-(3-propionic acid)-based peptidomimetic receptor that binds amphiphilic anionic guests in aqueous solution, Figure 2A.[44] The dibenzofuran-based template separates the covalently attached peptide strands by an average of 10 Å, allowing a peptide of complimentary structure (the $i + 1$ strand) to be bound between the i and $i + 2$ strands of the receptor, affording a three stranded antiparallel β-sheet at pH 5.75 (acetate buffer), Figure 2A. This host−guest 3-stranded β-sheet undergoes further assembly, apparently mediated by the anionic guest (neutralizes charge repulsion between cationic H·G complexes) yielding high molecular weight assemblies which ultimately become insoluble.

Peptidomimetic receptor **A** adopts a largely unordered structure in aqueous solution over the pH range of 3−10 in the absence of added guest. However, removal of + charge by adjusting the pH to >12 results in receptor dimerization (Figure 2B), yielding a four-stranded β-sheet which undergoes further assembly to form β-sheet quaternary structures that have gel-like properties. Interestingly, this pH induced assembly process is reversible by simply lowering the pH. Unfortunately, the high pH required for assembly (pH > 12) limits the utility of the peptidomimetic **A** for detailed studies.

For the purposes of this investigation, we have prepared a peptidomimetic analogous to **A**, peptidomimetic **B** (Figure 2), that undergoes spontaneous assembly over a wide pH range as a result of being composed largely of uncharged residues. Peptidomimetic **B** will be used to understand the environmental and structural features required to control β-sheet mediated quaternary structure formation. The ability to control the assembly pathway(s) and the final quaternary structure(s) afforded could prove to be particularly useful in deciphering the quaternary structural requirements for neurotoxicity associated with amyloid diseases and for the fabrication of polypeptide materials.

Results

Design and Synthesis of Peptidomimetic B. To prepare the collection of quaternary structures outlined in Figure 1, we anticipated that it would be necessary to reduce the charge on peptidomimetic **A**. The positively charged Lys residues were replaced by neutral Thr residues affording peptidomimetic **B**, Figure 2. Threonine was chosen for its high β-sheet propensity and its ability to improve the solubility of the quaternary structures formed in aqueous solution.[4,45] The *N*,*N*-dimethylethylenediamine (dmda) C-terminal substructures (Figure 2) were carried over from peptidomimetic **A** to further enhance

(29) Barrow, C. J.; Yasuda, A.; Kenny, P. T. M.; Zagorski, M. G. *J. Mol. Biol.* **1992**, 225, 1075−1093.
(30) Caughey, B.; Kocisko, D. A.; Raymond, G. J.; Lansbury, P. T., Jr. *Chem. Biol.* **1995**, *2*, 807−817.
(31) Sunde, M.; Serpell, L. C.; Bartlam, M.; Fraser, P. E.; Pepys, M. B.; Blake, C. C. F. *J. Mol. Biol.* **1997**, *273*, 729−739.
(32) Sunde, M.; Blake, C. C. F. *Q. Rev. Biophys.* **1998**, *31*, 1−39.
(33) Jimenez, J. L.; Guijarro, J. I.; Orlova, E.; Zurdo, J.; Dobson, C. M.; Sunde, M.; Sailbil, H. R. *EMBO. J.* **1999**, *18*, 815−821.
(34) Cohen, A. S.; Shirahama, T.; Skinner, M. In *Electron Microscopy of Amyloid*; Cohen, A. S., Shirahama, T., Skinner, M., Eds.; Academic Press: London, 1982; Vol. 3, pp 165−205.
(35) Serpell, L. C.; Sunde, M.; Fraser, P. E.; Luther, P. K.; Morris, E. P.; Sangren, O.; Lundgren, E.; Blake, C. C. F. *J. Mol. Biol.* **1995**, *254*, 113−118.
(36) Blake, C. C. F.; Serpell, L. C. *Structure* **1996**, *4*, 989−998.
(37) Harper, J. D.; Wong, S. S.; Lieber, C. M.; Lansbury, P. T., Jr. *Biochemistry* **1999**, *38*, 8972−8980.
(38) Maggio, J. E.; Mantyh, P. W. *Brain Pathol.* **1996**, *6*, 147−162.
(39) Malinchik, S. B.; Inouye, H.; Szumowski, K. E.; kirschner, D. A. *Biophys. J.* **1998**, *74*, 537−545.
(40) Blake, C. C. F.; Serpell, L. C.; Sunde, M.; Sandgren, O.; Lundgren, E. In *A Molecular Model of The Amyloid Fibril*; Blake, C. C. F., Serpell, L. C., Sunde, M., Sandgren, O., Lundgren, E., Eds.; John Wiley and Sons: Chichester, 1996; Ciba Symposium No. 199, pp 6−21.
(41) Kirschner, D. A.; Abraham, C.; Selkoe, D. J. *Proc. Natl. Acad. Sci. U.S.A.* **1986**, *83*, 503−507.
(42) Bauer, H. H.; Aebi, U.; Haener, M.; Hermann, R.; Mueller, M.; Arvinte, T.; Merkle, H. P. *J. Struct. Biol.* **1995**, *115*, 1−15.
(43) Arvinte, T.; Cudd, A.; Drake, A. F. *J. Biol. Chem.* **1993**, *268*, 6415−6422.
(44) LaBrenz, S. R.; Kelly, J. W. *J. Am. Chem. Soc.* **1995**, *117*, 1655−6.
(45) Minor, D. J.; Kim, P. S. *Nature* **1994**, *367*, 660−663.

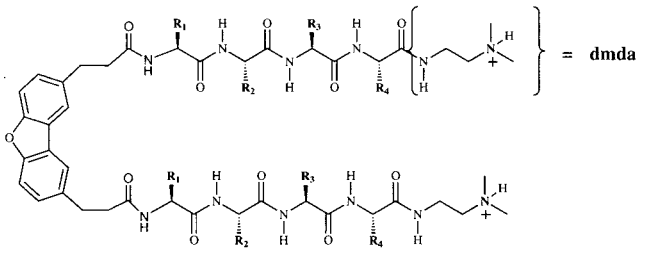

R_n = Residue-n

Peptidomimetic Receptor	Residue-1	Residue-2	Residue-3	Residue-4
A	Val	Lys	Leu	Lys
B	Val	Thr	Val	Thr

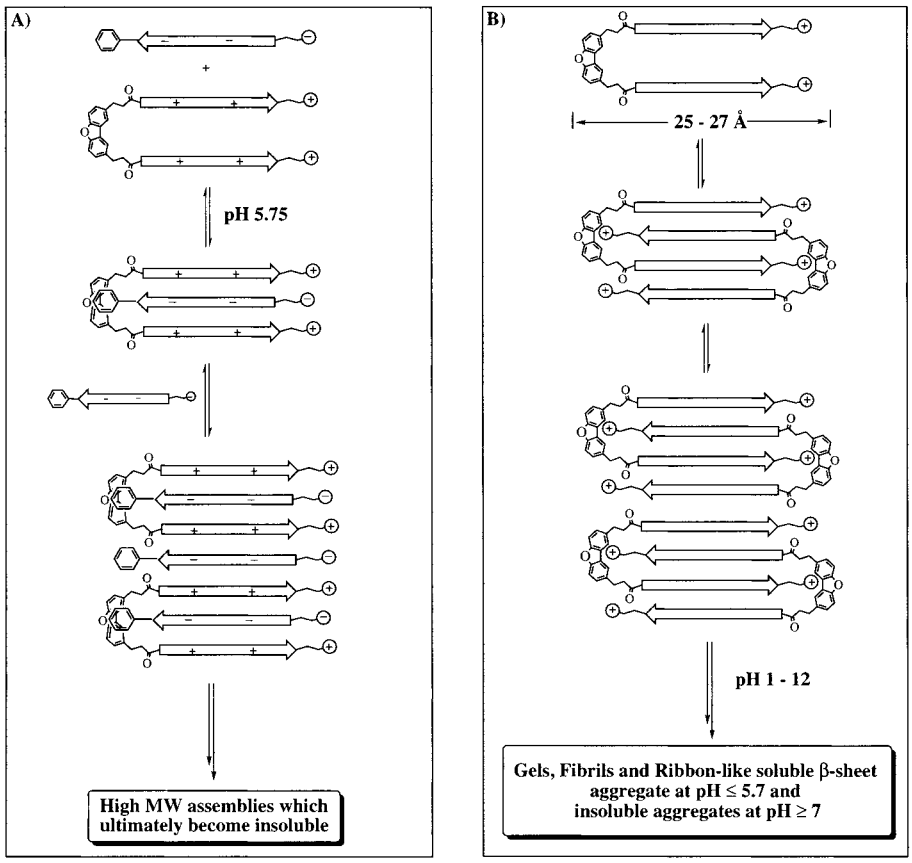

Figure 2. Schematic illustration of the 2,8-dibenzofuran-based peptidomimetics and their two proposed pathways of β-sheet quaternary structure formation: either through the binding of a complimentary guest followed by further assembly of the H·G complex mediated by the anionic guest (A) or through peptidomimetic dimerization via charge neutralization followed by further assembly (B) (lamellar assembly not shown).

the solubility of peptidomimetic **B** over a wide pH range (pK_a 10−11), owing to the charge of +1 that each of these residues is expected to carry in the unassembled state below pH 10 (overall charge of +2).

Peptidomimetic **B** is anticipated to have a width of 25−27 Å, based on CPK models, similar to the observed width of protofilaments of amyloid fibrils, Figure 2B (See Figure 14 for a molecular description of protofilaments). Its size coupled with its tendency to undergo intermolecular self-assembly provides hope that the collection of quaternary structures outlined in Figure 1 could be prepared. We anticipated that it may be possible to control the distribution of quaternary structures afforded by manipulating solution pH, ionic strength, and the like, owing to quaternary structural dependent perturbations of the pK_a of the dmda group. The dibenzofuran template is expected to preorganize peptidomimetic **B** for the formation of the four stranded β-sheet dimer (Figure 2B), which should further assemble into a monolayer cross β-sheet quaternary structure via H-bonding and hydrophobic interactions. The amphiphilicity of the strand sequence (VTVT) should strongly favor face to face packing (sandwich formation) of these assemblies at an intermediary assembly stage, affording a bilayer cross β-structure that is 25−27 Å wide and ∼10−12 Å high (protofilaments), see Figure 14. Further face to face packing (lamellae formation) beyond the bilayer stage is also possible. We expect that the protofilaments will undergo further assembly

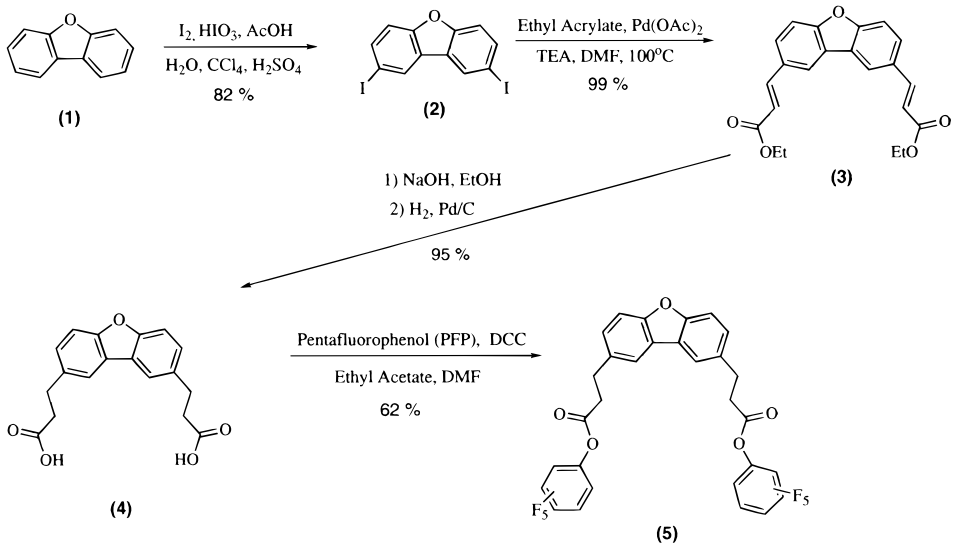

Figure 3. Outline of the synthesis of the dibenzofuran-based template precursor (2,8 -dibenzofuranbis(pentafluorophenyl-3-propionate) employed in solution phase peptide segment condensations.

into filaments via edge to edge assembly of protofilaments favored by the hydrophobic interactions between the templates (see Figure 14) or by a strand swapping mechanism (see discussion and Figure 15). The filaments should then self-assemble into fibrils (Figure 1B), ribbons (Figure 1C) and possibly tube-like assemblies (Figure 1E), again through edge to edge packing driven by the hydrophobic effect and /or strand swapping.

The synthesis of the peptidomimetic **B** commenced with the preparation of the template (2,8-dibenzofuran-bis-(3-propionic acid)) outlined in Figure 3. Electrophilic aromatic iodination of dibenzofuran **(1)** gave 2,8-diiododibenzofuran **(2)** in 82% yield.[46] Intermediate **2** was subjected to a tandem palladium catalyzed Heck cross-coupling reaction with ethyl acrylate affording the bis-α-*β*-unsaturated ethyl ester 2,8-dibenzofuran-bis-(ethyl-3-propionate) **(3)** in 99% yield.[47−49] Saponification followed by hydrogenation of diester **3** affords the C_2 symmetric 2,8-dibenzofuran-bis-(3-propionic acid) **(4)** in 95% yield.[50] Diacid **(4)** was converted to 2,8-dibenzofuran-bis-(pentafluorophenyl-3-propionate) **(5)** in 62% yield (after recrystallization) employing a dicyclohexylcarbodiimide (DCC) mediated esterification with pentafluorophenol. The total yield of **5** from dibenzofuran **1** was 48%.

The side-chain-protected peptide strands utilized in the synthesis of peptidomimetic **B** were assembled on oxime solid-phase resin (R_{ox}) using a t-Boc strategy. The peptide was synthesized by attaching the carboxyl group of Nα-*t*-Boc-benzyl (bzl)-protected-threonine to the oxime resin, Figure 4A. The peptide was then elongated in a stepwise manner to afford R_{ox}-Thr(bzl)-Val-Thr(bzl)-Val-*t*-Boc using the methodology described by Chitnumsub.[51] Cleavage of the side-chain-protected peptide from the oxime resin was accomplished by the nucleophile *N,N*-dimethylethylenediamine (dmda) yielding the protected peptide **(6)**, Figure 4A.[52−57] The N-terminal Boc protecting group was removed using a 1:3 TFA/CH_2Cl_2 solution, and the peptide was purified by C_{18} RP-HPLC affording the TFA salt of **(6)**. Peptidomimetic **B** was synthesized by mixing 2,8-dibenzofuran-bis-(pentafluorophenyl-3-propionate) **(5)** and the side-chain-protected peptide segment TFA·H_2N-Val-Thr-(bzl)-Val-Thr(bzl)-dmda **(6)** in DMF (Figure 4B).[56,58] The reaction was initiated via addition of DIEA, ensuring that sufficient quantities were added to make the DMF coupling solution slightly basic (pH 7−10) when applied to prehydrated pH paper. The time course of the coupling reaction was monitored by RP-HPLC. Side chain deprotection of the benzyl-based protecting groups was accomplished by catalytic hydrogenation in the presence of 10% Pd/C in a mixture of formic acid and methanol (∼2:1).[59] Purification by RP-HPLC yielded peptidomimetic **B** (**8**) in > 98% purity as confirmed by C_{18} RP-HPLC and ESI/MS ($M + H_{calcd} = 1253.5$, $M + H_{obsd} = 1254.0$ g/mol), 45% overall yield.

Solution Properties of Peptidomimetic B. The tertiary ammonium groups on the C-termini of strands *i* and *i* + 2 and the two Thr residues within each strand confer good solubility on peptidomimetic **B** in aqueous solution over a wide pH range (pH 1−10) at a concentration up to 2 mM, above which translucent gel-like assemblies formed.[2] Concentration dependent circular dichroism spectra of peptidomimetic **B** in water (pH 5−6) incubated at room temperature for 24 h are shown in Figure 5A. Over the concentration range of 50−200 μM the peptide displayed far-UV CD spectra indicative of an ensemble of largely unordered conformations. Sedimentation equilibrium studies on peptidomimetic **B** (50 μM, 24 h, pH 6 not buffered) in water yielded an average molecular weight of 1281

(46) Schwartz, E. B.; Knobler, C. B.; Cram, D. J. *J. Am. Chem. Soc.* **1992**, *114*, 10775−10784.
(47) Wirth, H. O.; Waese, G.; Kern, W. *Makromol. Chem.* **1965**, *86*, p139.
(48) Heck, R. F. *Palladium Reagents in Organic Syntheses*; Academic Press: London, U.K. 1985.
(49) Ziegler, C. B., Jr.; Heck, R. F. *J. Org. Chem.* **1978**, *43*, 2941−2946.
(50) Hartung, W. H.; Simonoff, R. *Organic Reactions*; John Wiley and Sons: New York, 1953; Vol. VII.
(51) Chitnumsub, P.; Fiori, W. R.; Lashuel, H.; Diaz, H.; Kelly, J. W. *Bioorg. Med. Chem.*, **1999**, 7, 39−59.
(52) DeGrado, W. F.; Kaiser, E. T. *J. Org. Chem.* **1980**, *45*, 1295−1300.
(53) DeGrado, W. F.; Kaiser, E. T. *J. Org. Chem.* **1982**, *47*, 3258−3261.
(54) Lansbury, P. T., Jr.; Hendrix, J. C.; Coffman, A. I. *Tetrahedron Lett.* **1989**, *30*, 4915.
(55) Hendrix, J. C.; Jarrett, J. T.; Anisfeld, S. T.; Lansbury, P. T., Jr. *J. Org. Chem* **1992**, *57*, 3414−3420.
(56) Kaiser, E. T.; Mihara, H.; Laforet, G. A.; Kelly, J. W.; Walters, L.; Findeis, M. A.; Sasaki, T. *Science* **1989**, *243*, 187−192.
(57) Lobl, T. J.; Maggiora, L. L. *J. Org. Chem.* **1988**, *53*, 1979−1982.
(58) Kisfaludy, L.; Low, M.; Nyeki, O.; Szirtes, T.; Schoen, I. *Liebigs Ann. Chem.* **1973**, 1421−1429.
(59) Pallenberg, A. J. *Tetrahedron. Lett.* **1992**, *33*, 7693−7696.

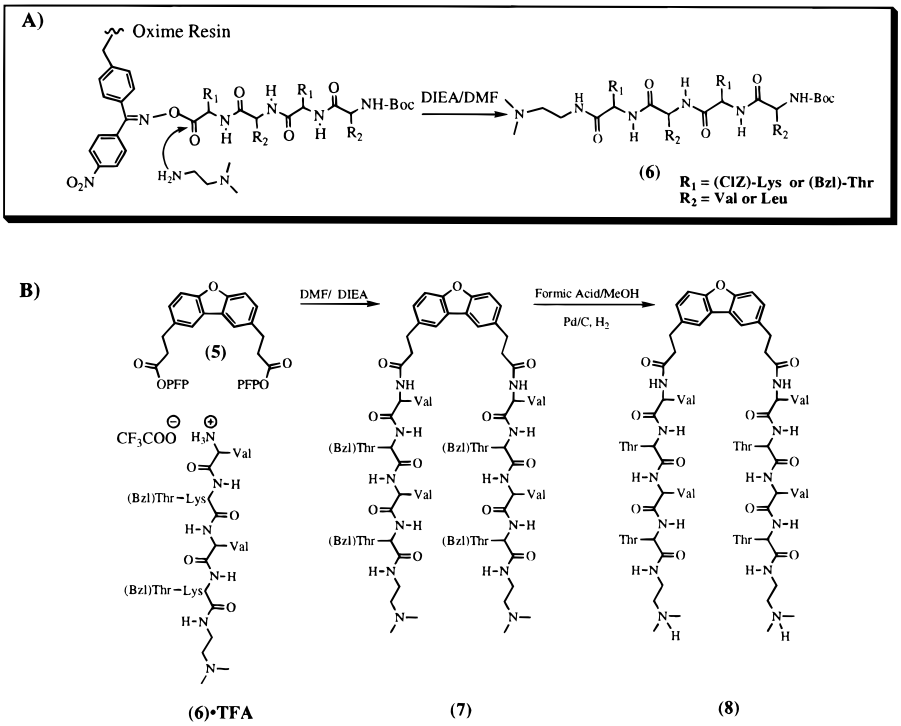

Figure 4. (A) Outline of the synthesis of the protected peptide segments on oxime resin and their cleavage from the oxime resin using the nucleophile dmda (*N*,*N*-dimethylethylenediamine). (B) Synthesis of peptidomimetic **B** (**8**) via a solution phase segment condensation reaction.

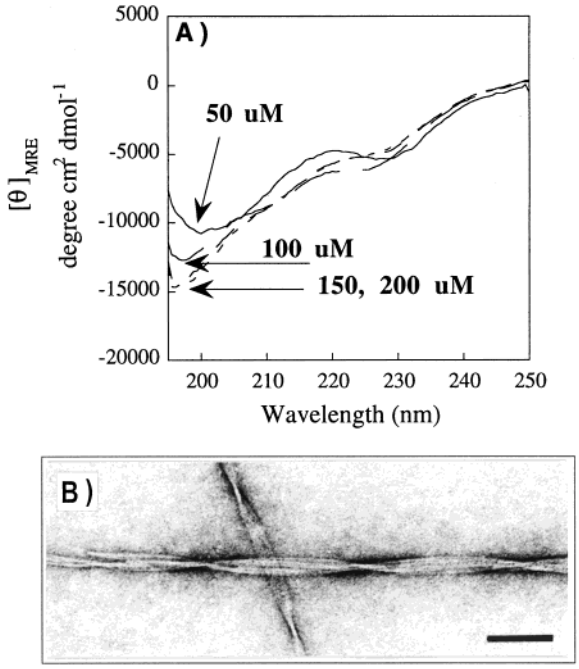

Figure 5. (A) Concentration dependent (50−200 μM) far-UV CD spectra of peptidomimetic **B** in distilled water (pH 5−6) incubated for 24 h. (B) Electron micrograph of a peptidomimetic **B** fibril (0.5 mM in water, pH $\approx$ 5−6) deposited onto a carbon coated EM grid after two weeks of incubation at 25 °C. The scale bar = 100 nm.

g/mol (calculated = 1254 g/mol), which corresponds to that of a monomer in solution, Supporting Information Figure 1.

Examination of stock solutions of peptidomimetic **B** dissolved in water (0.5 mM, pH $\approx$ 5−6) after 2 weeks of incubation at room temperature produced very viscous solutions, making CD spectral acquisition problematic. However, negatively stained electron micrographs of peptidomimetic **B** adsorbed to a hydrophobic EM grid revealed that it had undergone self-assembly into two-filament fibrils with a diameter of 100−130 Å (not shown) and four-filament fibrils characterized by a diameter of 240 Å, reminiscent of amyloid fibrils extracted from patients with amyloid disease, Figure 5B. Fraying at the ends of the fibril displayed in Figure 5B provides evidence for the association of two 100−130 Å two-filament fibrils to afford the four-filament helical fibrils. The four-filament fibrils exhibit a helical repeat of ~200 nm, that is, the distance between helical crossovers in the fibril structure, while the variable is approximately 200 nm. Filaments (50−60 Å, Figure 1A, 14) were rarely observed under these conditions. Unlike the fibrils formed by peptidomimetic **A** which precipitate, the fibrils formed by peptidomimetic **B** remain soluble and stable in water for up to 1 year when grown at a peptidomimetic concentration of 50−200 μM. Peptidomimetic **B** assembled in water as outlined above would be classified as amyloid based on EM morphology and their ability to bind thioflavin T, an amyloid selective dye, Supporting Information Figure 2.

To further characterize the fibrilar structure of peptidomimetic **B**, X-ray fiber diffraction studies were carried out on fibrils grown in water (pH 5−6, 1 mM) where soluble fibrils were evident within 10 h. Fibrils partially aligned in a magnetic field showed a considerable degree of orientation and revealed the classical cross-β diffraction pattern displayed by amyloid fibrils, Figure 6.[31,35,60,61] The intense 4.76 Å reflection corresponds to the spacing between hydrogen bonded β-strands which run perpendicular to the fibril axis (Figure 1A), while the more diffuse equatorial reflection at 9.7 Å corresponds to the spacing between the sheets of the bilayer or multilayer (see Figure 14).

Hydronium ion concentration has a dramatic effect on the rate of peptidomimetic **B** self-assembly. Over the pH range of 3−6 (50 mM acetate, no added salt) peptidomimetic **B** undergoes slow intermolecular association (by far-UV CD),

(60) Eanes, E. D.; Glenner, G. G. *J. Histochem. Cytochem.* **1968**, *16*, 673−677.
(61) Inouye, H.; Fraser, P. E.; Kirschner, D. A. *Biophys. J.* **1993**, *64*, 502−519.

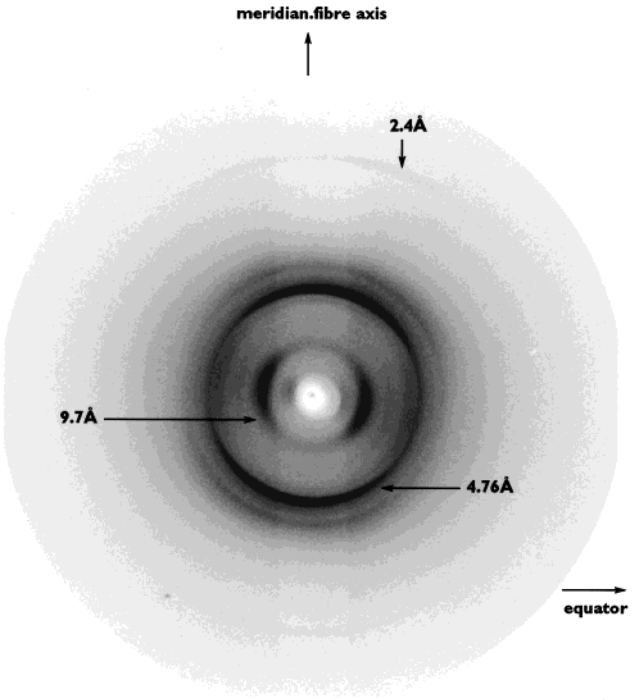

Figure 6. X-ray fiber diffraction pattern of magnetically oriented fibrils derived from a 1 mM solution of peptidomimetic **B** in water. The intense 4.76 Å meridional reflection corresponds to the spacing between hydrogen bonded β-strands which run perpendicular to the fibril axis, while the more diffuse equatorial reflection at 9.7 Å corresponds to the spacing between the sheets of the bilayer or multilayer. The 2.4 Å reflection on the meridian is the harmonic of the 4.76 Å reflection.

affording fibrils after several weeks of incubation. The addition of 50−100 mM NaCl to the buffered solutions was found to enhance the rate of peptidomimetic **B** assembly over the pH range of 3−6, allowing for fibril formation within 24 h. An increase in pH (7−10, 50 mM phosphate or carbonate−bicarbonate buffer, no added salt) produces a dramatic increase in the rate of quaternary structure formation, yielding a mixture of soluble and insoluble high MW β-sheet rich assemblies within a few minutes. The pH effect is likely the result of charge removal or lack thereof from the dmda groups as a consequence of the assembly mediated pK_a shifts at the C terminus of each strand.

To evaluate the effect of pH on the morphology of the quaternary structures formed, electron microscopy studies were carried out on peptidomimetic **B** in the presence of 75 mM NaCl (25 °C). Incubation of peptidomimetic **B** at pH 4.8 (50 mM acetate buffer) for two weeks yielded predominately two-filament fibrils having a diameter of 100−130 Å, Figure 7A. One four-filament 240 Å wide fibril was also observed on the grid, in addition to the 25 Å diameter protofilaments that can be seen in the background. Filaments (50−60 Å) composed of two protofilaments were rarely observed in this sample. Interestingly, individual fibrils differ in their degree of twist and the helical periodicity. Even within a fibril, the degree of twist and periodicity can vary dramatically.

At pH 5.7 (75 mM NaCl in 50 mM acetate buffer) morphologically distinct ribbon quaternary structures of peptidomimetic **B** are afforded instead of fibrils, Figure 7B. These ribbon structures appear to be composed of largely untwisted laterally associated filaments, presumably stabilized through hydrophobic interactions between the dibenzofuran substructures composing the filaments. The ribbon-based assemblies are composed of 3−36 filaments, where the average diameter of the individual filament in these assemblies is approximately 65

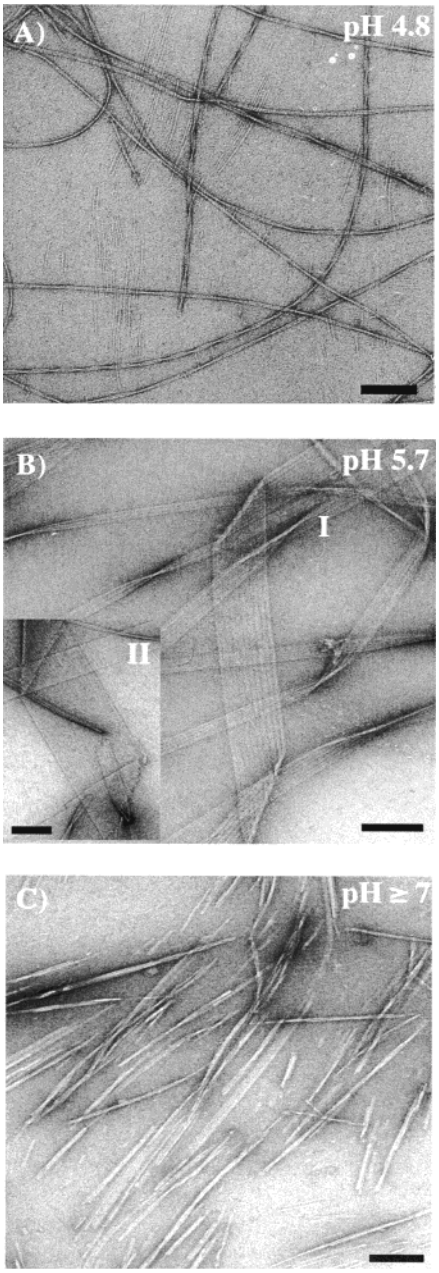

Figure 7. The effect of pH on quaternary structures formed by peptidomimetic **B** as evaluated by electron microscopy using negative staining from a solution of peptidomimetic **B** (50 μM) at pH 4.8 (A) and pH 5.7 (B) in acetate buffer (50 mM acetate, 75 mM NaCl) after incubation for 2 weeks at 25 °C. The inset in (B) is an electron micrograph of peptidomimetic **B** (50 μM) at pH 5.7 in acetate buffer (50 mM acetate, 75 mM NaCl) after 3 months of incubation at 25 °C. (C) Electron micrographs of peptidomimetic **B** (50 μM) at pH 7.0 in phosphate buffer (50 mM phosphate and 75 mM NaCl). For all micrographs, the scale bars represent 100 nm.

Å. The apparent twist observed in the micrographs is highly variable and may be caused by the hydrophobic interactions between the grid and the planar ribbon structures (Figure 7B, **I**). The kinks and apparent fragmentation observed support this interpretation. Interestingly, two-filament ribbons of 100−130 Å were rarely observed at pH 5.7. Ribbons composed of greater than three filaments remain as the predominant quaternary structure even after 1 year of incubation, indicating that they are the thermodynamic product or a kinetic product having insurmountable kinetic barriers for conversion to alternative structures.

At pHs ≥ 7 (50 mM phosphate buffer, 75 mM NaCl) peptidomimetic **B** self-assembles into a heterogeneous array of quaternary structures including rods, Figure 7C. Presumably, the rate of assembly is higher than that observed at lower pH and specificity suffers due to nonspecific hydrophobic interactions mediated by deprotonation of the dmda groups-owing to quaternary structure dependent pK_a shifts. Alternatively, the phosphate counterion may interact with the ammonium groups through electrostatic interactions interfering with assembly specificity. The rods appear to have an aircraft cable type structure, apparently composed of various numbers of protofilaments and filaments. There are numerous defects in these rods. They also exhibit drastically different extents of twist, possibly because under these conditions the protofilaments can add to each other and progress beyond the filament stage, as apparent from the ragged ends. Changes in the ionic strength of the solution do not appear to significantly alter the quaternary structural distribution produced at pHs ≥ 7.

All the quaternary structures formed over the pH range of 1−12 (50−100 mM NaCl) (including protofilaments, filaments, fibrils, ribbons, and rods or cables) bind the amyloid selective dyes Congo red and thioflavin T, similar to the behavior of amyloid proteins found in fibrous deposits within amyloid patients, Supporting Information Figure 3. Evidence is strong for the ability of both soluble quaternary structures of varying morphology (pH < 7) and visually perceptible aggregates (pH ≥ 7) to bind Congo red and thioflavin T. Hence it is highly unlikely that dye binding alone will be able to distinguish between the numerous possible quaternary structures observed and to identify those that have neurodegenerative properties.

Characterization of Peptidomimetic B Assemblies by Atomic Force Microscopy. The commercially available silicon tips used for AFM imaging have an average end radii of curvature of ∼10 nm. This precludes accurate determination of the diameter of fibrilar quaternary structures which are ≤100 Å wide, thus the width of the protofilaments and filaments would be exaggerated by convolution, especially since filaments and ribbons of peptidomimetic **B** appear to be more flat, rather than cylindrical, Figure 8A.[62] However, accurate height measurements are still possible with such tips. Atomic force microscopy reveals ribbons of peptidomimetic **B** formed in solution (pH 5.7) after 3 months of incubation. The long ribbons have an average height of 31 Å (Figure 8B, **a**) and appear to be four-β-sheets thick (two bilayers). Two additional species can be detected, single ribbons with an average height of 23 Å (Figure 8B, **b**) are fairly rare and appear to be three-β-sheets thick while numerous small quaternary structures with an average height of 11 Å (Figure 8B, **c**) predominate. The presence of quaternary structures of 11 Å in height in the background is consistent with the detection of filament quaternary structural intermediates which are also observed by EM at both pH 4.8 and 5.7 (Figure 7A, B, 9A). The 11 Å height is consistent with the calculated height of a β-sheet bilayer-two β-sheets stacked in a face to face manner, presumably interacting through the Val residues to form a β sandwich, see Figure 14.

Unfortunately fibril-like assemblies (two and four filament helical fibrils) observed at pH 4.8 by EM did not adsorb well to the mica surface and could not be examined by AFM at this time. However, AFM images of peptidomimetic **B** quaternary structures that do adsorb to the mica surface at pH 4.8 reveal predominantly short assemblies with an average height of 6 Å

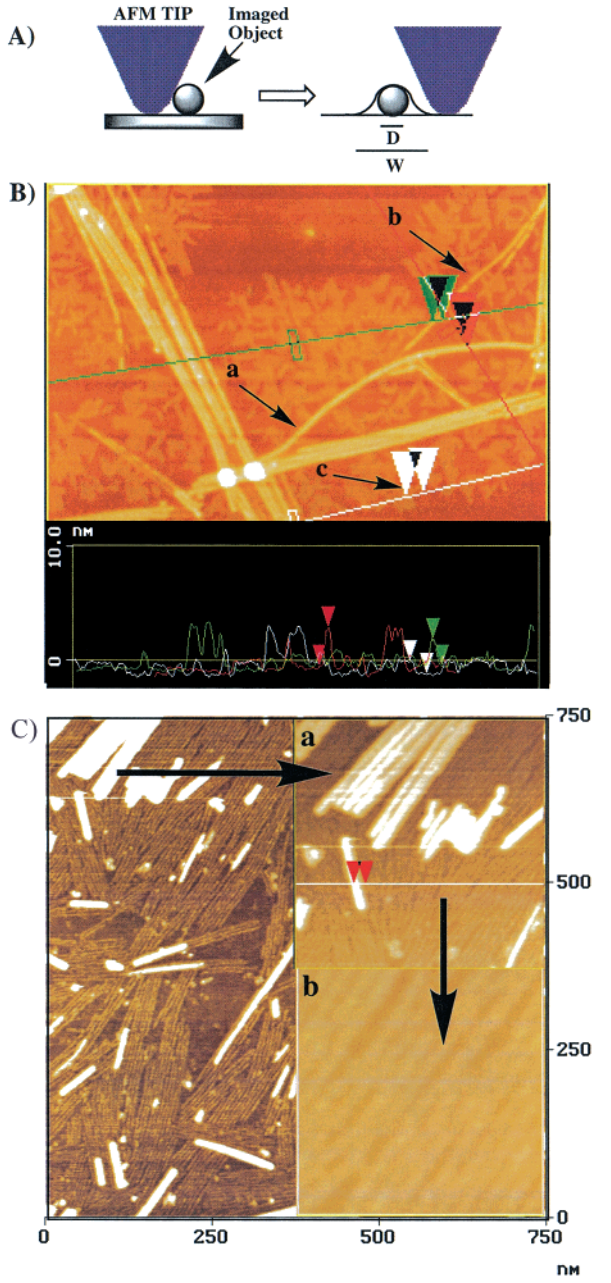

Figure 8. (A) A schematic representation showing the deflections caused by the interaction of the AFM silicon tip with the surface of the sample, illustrating why the height of a sample can be determined with accuracy unlike the width of the sample. The measured width W is larger than the actual width D owing to the size of the tip relative to the quaternary structure of peptidomimetic **B**. The degree of width overestimation is related to the shape and width of the silicon tip which changes during the measurement (B) Atomic force microscopy images of peptidomimetic **B** (50 μM) at pH 5.7 absorbed to a mica surface from acetate buffer (50 mM acetate, 75 mM NaCl) after incubation for 3 months at 25 °C. The ribbons labeled a, b, and c have average heights of 31, 23 and 11 Å, respectively. The triangles on the colored straight lines shown above reflect the difference in height between the background and the indicated quaternary structures in **B**. (C) Atomic force microscopy images (tapping mode) of peptidomimetic **B** adsorbed to mica from solution at pH 4.8 in acetate buffer (50 mM acetate, 75 mM NaCl) after incubation for 3 months at 25 °C dried onto a mica surface. The inset figures **a** and **b** illustrate a magnified view of the quaternary structures (identified by the black arrows). A mixture of quaternary structures with an average height of 6 and 30 Å in **a** and mainly 6 Å high quaternary structures in **b** is revealed.

(62) Harper, J. D.; Wong, S. S.; Lieber, C. M.; Lansbury, P. T., Jr. *Chem. Biol.* **1997**, *4*, 119−125.

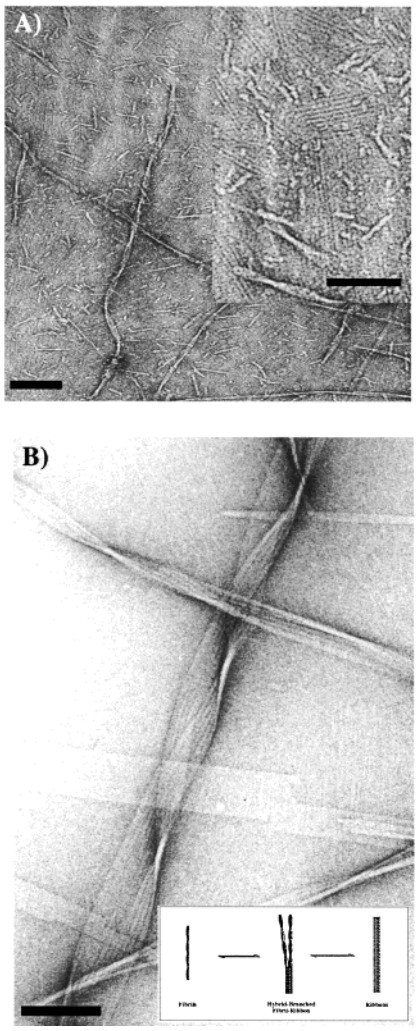

Figure 9. (A) Electron micrographs of negatively stained quaternary structures deposited from a solution of peptidomimetic **B** (50 μM) at pH 4.8 in acetate buffer (50 mM acetate, 75 mM NaCl) after incubation for 20−30 h at 25 °C. (B) Electron micrographs of negatively stained quaternary structures deposited from a solution of peptidomimetic **B** (50 μM) at pH 5.7 in acetate buffer (50 mM acetate, 75 mM NaCl) after incubation for 2 months at 25 °C demonstrating the coexistence of fibrils and ribbon assemblies, implying the latter come from the former. For all micrographs, the scale bar = 100 nm.

and a minor population of species with an average height of 31 Å (Figure 8C, **a**). The measured average height of the short assemblies of 6 Å corresponds to the height of a single peptidomimetic **B** monolayer (Figure 8C, **b**), assembled by hydrogen bonding but not stacked into a bilayer.

Characterizing the Assembly Pathway of Peptidomimetic B into Fibrilar Structures by Electron Microscopy and Analytical Ultracentrifugation. Time Course EM Studies. To gain insight into the mechanism of fibril formation by peptidomimetic **B** we followed its assembly as a function of time by electron microscopy and analytical ultracentrifugation methods. Early electron micrographs of peptidomimetic **B** (50 μM, 20−30 h, in 50 mM acetate, 75 mM NaCl) over the pH range of 3.4−4.8 revealed that it had undergone self-assembly to form predominantly two types of quaternary structures: protofilaments (25−27 Å wide, with an average length of 35 nm) and short 60 Å wide filaments (composed of two protofilaments), Figure 9A. Fibrils composed of two filaments (100−130 Å in width) and four-filament fibrils (240−260 Å in width) are present as minor species (<10%). A major change in the distribution of quaternary structures present in solution, favoring the latter species, is evident after two weeks of incubation at 25 °C as shown previously in Figure 7A.

The 25 Å wide protofilaments were always present surrounding the fibrils early in the time course and seem to significantly decrease in representation in samples that contained fibrils at later stages of assembly (two- to four-filament fibrils (100−260 Å) are the major species). These data and the AFM results suggest that the 25 Å protofilaments are the precursors to the filaments that further assemble into amyloid fibrils, however this has not been proven. In some cases the average length of the 60 Å wide filaments was similar to that exhibited by the surrounding two-filament fibrils (200−500 Å) suggesting that initiation of fibril formation does not necessarily require the formation of long unbranched filaments. However, we cannot rule out the possibility that these short 60 Å filaments could result from the fragmentation of two-filament fibrils during sample drying on the EM grid. The results outlined above suggest that protofilaments, filaments and fibrils represent quaternary structures of increasing complexity and are composed of common building blocks or microstructures.

An equilibrium may exist between *n*-filament helical fibrils and flat ribbons at pH 5.7 (50 mM acetate, 25 °C, incubation period of 3 months), Figure 9B. The electron micrograph illustrates two ∼400 Å wide fibril assemblies (5-filaments each), merging together to form a flat ribbon assembly that is 10-filaments wide (820 Å). Under these conditions it appears that fibrils afford ribbons as the former are the dominant quaternary structure at early time points (2 weeks, Figure 7A), while the latter are stable for incubation periods of 3 months to a year. This is not an isolated observation, similar species were regularly observed during our studies at this pH.

Characterizing the Distribution of Quaternary Structures in Solution by Analytical Ultracentrifugation. Analytical ultracentrifugation methods were employed to assess the aggregation state of peptidomimetic **B** under conditions where self-assembly was detected by electron microscopy. Experiments were carried out with peptidomimetic **B** (50 μM) at pH 3.4, 4.4 and 5.7 (50 mM acetate buffer, 100 mM NaCl). Under these conditions two types of species were observed: a soluble high molecular weight fast sedimenting quaternary structure (sediments completely within an hour at 20,000 rpm) and a low molecular weight nonsedimentable species (monomer, see below) implied by the nonzero baseline (Figure 10A). The soluble quaternary structures exhibit sedimentation coefficients ranging from 60 to 105 S (MW > 500 KDa), consistent with a heterogeneous distribution of assemblies. Approximately 37, 45, and 20% of unsedimented peptidomimetic **B** is left in solution at pHs 3.4, 4.7, and 5.7, respectively (based on absorbance). Equilibrium studies were performed at 50 000 rpm to characterize the low MW species which corresponds to a single ideal species of MW 1190−1279 Da over the pH range of 3−5.7, consistent with monomeric peptidomimetic **B**, Figure 10B. The far-UV CD spectrum of this sample is consistent with a largely unstructured peptidomimetic **B** (Figure 10C), congruent with its monomeric nature. Sedimentation velocity studies on peptidomimetic **B** studied at pHs ≥ 7 at 3000 rpm resulted in rapid sedimentation of >95% of the sample to the bottom of the cell.

Dependence of Peptidomimetic B β-sheet Formation and Self-Assembly on Solution Conditions. The X-ray fiber diffraction data suggest that peptidomimetic **B** assemblies are rich in β-sheet structure, Figure 6. An increase in β-sheet quaternary structure as a function of pH and ionic strength was monitored by circular dichroism via the reduction of the random

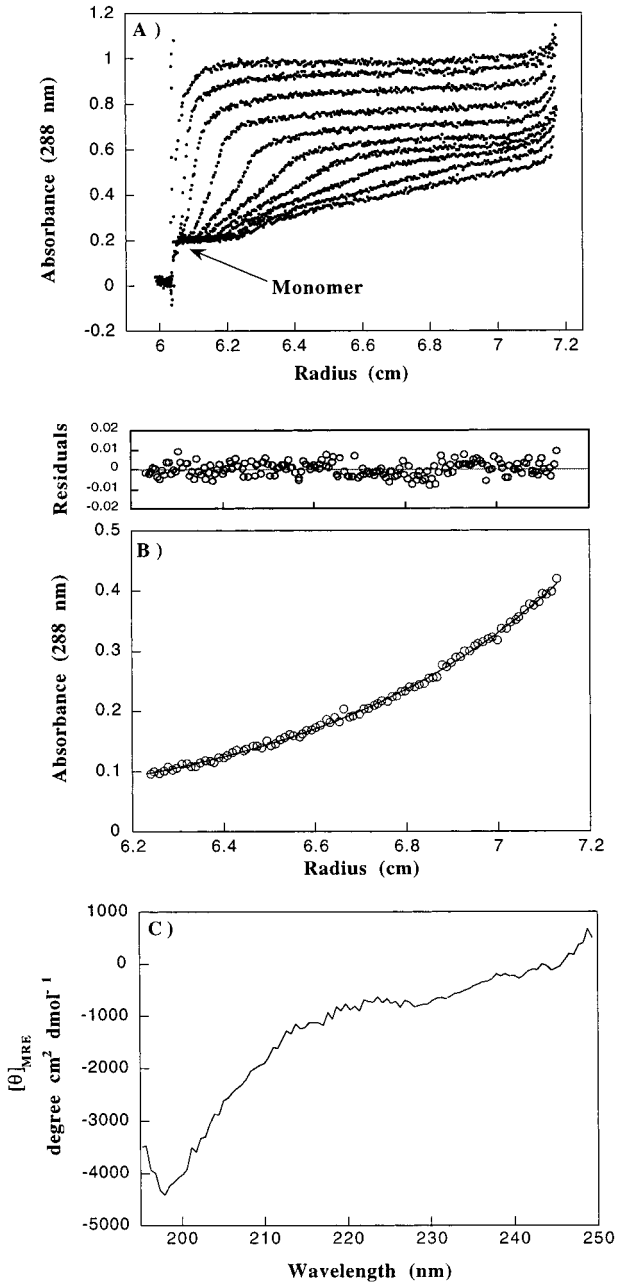

Figure 10. (A) Sedimentation velocity profile of peptidomimetic **B** (50 μM) at pH 5.7 (50 mM acetate, 75 mM NaCl) after incubation at 25 °C for two months, revealing the presence of a heterogeneous distribution of high MW peptidomimetic **B** aggregates, which sediment within an hour at 20 000 rpm in the analytical ultracentrifuge. Scans were acquired at 1-min intervals; for clarity scans every 2 min are shown. The absorbance baseline at 0.22 absorbance units represents unsedimented peptidomimetic **B** (B) Sedimentation equilibrium analysis of the remaining peptidomimetic that did not sediment during the course of the velocity experiment affords an absorbance distribution profile which gives an excellent fit to a single ideal species model as judged by the residuals (difference between the experimental data and the fitted data for each point) yielding a molecular weight of 1234 g/mol which corresponds to the calculated molecular weight of peptidomimetic **B** monomer (1254 g/mol). (C) Far-UV CD spectrum of the unsedimented monomeric peptidomimetic **B**, consistent with a largely unordered conformation.

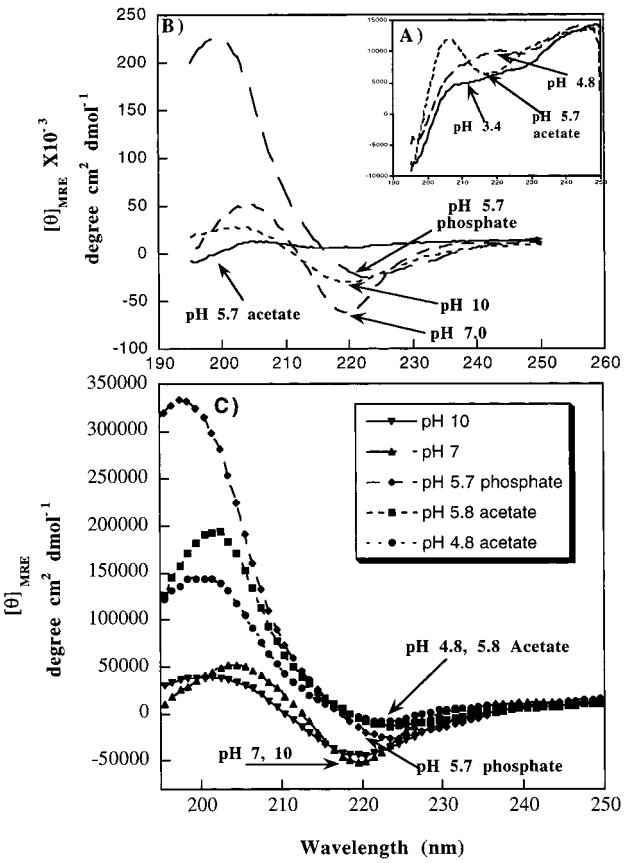

Figure 11. pH dependent far-UV CD spectra of peptidomimetic **B** (50 μM) in the absence of NaCl (A,B) and in the presence of 50 mM NaCl (C). All spectra were recorded after 24 h of incubation at 25 °C. Solutions of peptidomimetic **B** (50 μM) were prepared by diluting peptidomimetic **B** (0.5−1 mM in water) employing the following buffers: 50 mM of acetate buffer (at pH 3.4, 4.8 and pH 5.7), phosphate buffer (at pH 5.7, and pH 7.0), and carbonate−bicarbonate buffer at pH 10.

coil signal (minimum at 195 nm) and the growth of the characteristic β-sheet quaternary structure spectrum (minimum at 215−222, maximum at 195 nm) after 24 h of incubation. Far-UV CD analysis of peptidomimetic **B** (50 μM) over the pH range of 3−6 (50 mM acetate, no added NaCl) demonstrates that it adopts a predominantly random coil structure, as discerned by the dominant minimum at 195 nm, Figure 11A. Sedimentation equilibrium data on peptidomimetic **B** (50 μM) after 24 h of incubation at room-temperature fits well to a single ideal species model, yielding average molecular weights of 1190 and 1234, at pH 4.8 and 5.7, respectively. At pHs $\geq$ 7 (in phosphate, carbonate−bicarbonate buffers) peptidomimetic **B** exhibits a signal that is characteristic of an assembled β-sheet structure with a broad minimum at 220 nm and maximum at 200−205 nm, indicating that the transition from coil to assembled β-sheet structure occurs within 24 h at higher pH, Figure 11B.

The observed solution properties of peptidomimetic **B** were evaluated at constant pH in phosphate and acetate buffers to evaluate the role that buffers may play in β-sheet mediated quaternary structure formation. A comparison of acetate and phosphate buffers at pH 5.7 (no added salt) demonstrated that phosphate efficiently induces a random coil to β-sheet quaternary structural transition after 24 h of incubation (evident by the disappearance of the 195 nm minimum and the appearance of minimum at 223 nm and a maximum at 195 nm), Figure 11B. The same time dependent evaluation of peptidomimetic **B** in acetate buffer pH 5.7 yields a random coil structure, Figure 11B.

The addition of NaCl (50 mM) to peptidomimetic **B** at low pH afforded a transition from random coil to a β-sheet quaternary structure at pHs <6 (50 mM acetate, 24 h preincubation), Figure 11C. A correlation exists between the increase

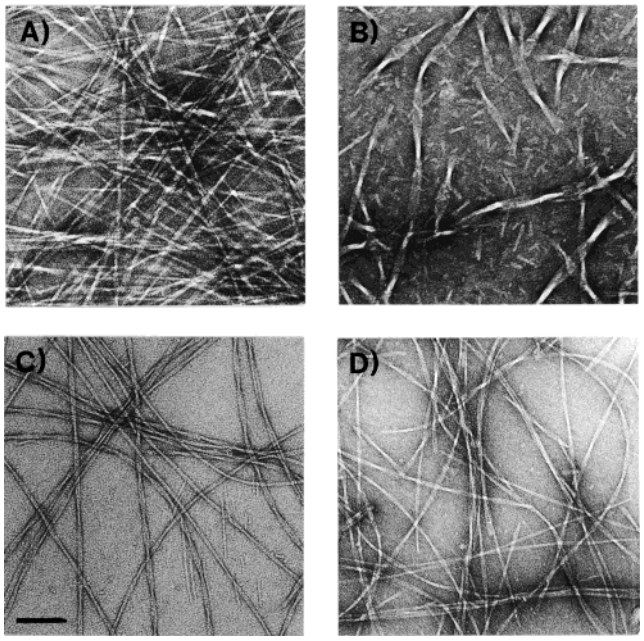

Figure 12. Electron micrographs of negatively stained fibrils deposited from peptidomimetic **B** D_2O solutions at pD1 (A), pD 4 (B), pD 8.4 (C), and pD 12 (D). The scale bar shown in C (100 nm) applies to A, B, and D.

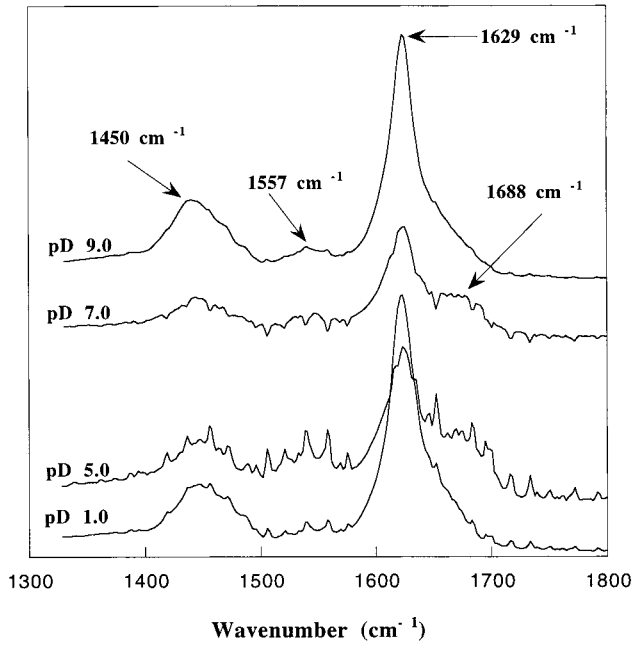

Figure 13. Thin film FT-IR spectra in the amide I and amide II region of peptidomimetic **B**, obtained by drying solutions of peptidomimetic **B** (50 μM in D_2O) at pD 1, 5, 7 and 9. The dominant band at 1629 cm^{-1} is characteristic of a β-sheet conformation, and the shoulder band at 1688 cm^{-1} is characteristic of antiparallel β-sheet structures.

in β-sheet structure and the enhanced rate of peptidomimetic **B** self-assembly exhibited upon addition of 50−100 mM NaCl over the pH range of 3−6. At pHs ≥ 7 (in phosphate and carbonate−bicarbonate buffers), peptidomimetic **B** aggregation (90−95%) was not noticeably effected by addition of NaCl (50−200 μM), suggesting that more dramatic effect of pH and buffer composition on sheet-mediated assembly may make the salt effect difficult to detect, which is dramatic at low pH. Far-UV CD of the unsedimented soluble peptide exhibited a weak minimum at 220 nm with no random coil signal, suggesting that the coil-to-β-sheet equilibrium is shifted toward β-sheet quaternary structure formation at pH 7 by addition of NaCl, Supporting Information Figure 4.

The Effect of Solution Components on Peptidomimetic B Fibril Morphology. Samples of peptidomimetic **B** (50 μM) in D_2O over the pD range of 1−12 (the pD of the samples were adjusted using DCl and NaOD) were incubated for two weeks at room temperature to probe whether assembly could occur at low ionic strength. Electron micrographs reveal the formation of several pH-dependent, morphologically distinct quaternary structures, Figure 12. All solutions over the pD range of 1−12 produced fibrilar structures after two weeks. Four main categories of species were observed: protofilaments (25 Å) in width, flat and twisted filaments 50−60 Å in width, 100−130 Å two-filament fibrils, and highly ordered four-filament helical fibrils with an average diameter of 240−260 Å (all quaternary structures bound to thioflavin T and Congo red (data not shown)). Peptidomimetic **B** forms two-filament fibril structures at pD1 (Figure 12A) whereas, four-filament helical fibrils (240−260 Å in diameter) were dominant over the pD range 4−6 (Figure 12B). Over the pD range of 7−10, a mixture of tightly associated 130 Å two-filament helical fibrils and loosely associated 60 Å filaments were found to predominate (Figure 12C). Extensive aggregation (85% − 95% by analytical ultracentrifugation) was observed over the pD range of 10−12, where the dominant soluble assemblies were two-filament fibril structures (100−130 Å), with a minor population of four-filament fibril structures (240−260 Å), (Figure 12D). The high pH solutions exhibit turbidity at 330 nm, suggesting the formation of large aggregates and precipitates.

Fourier Transform Infrared Spectroscopy (FT-IR) Analysis of Peptidomimetic B as a Function of pH. The secondary structure of the assemblies formed by peptidomimetic **B** in D_2O as a function of pH were evaluated by infrared spectroscopy using the same samples subjected to evaluation by electron microscopy, Figure 12. Evaporation of the aqueous solution (preincubated for two weeks) on a CaF_2 plate produced a transparent film, which yielded the infrared spectra shown in Figure 13. The conformation sensitive amide I band exhibited a spectrum characteristic of an antiparallel β-sheet structure with a strong absorption centered at 1629 cm^{-1} with a weak band at 1688 cm^{-1} for peptidomimetics incubated over the pD range of 1−12, Figure 13. The amide II band centered at 1557 cm^{-1} in H_2O is very weak and appeared to be shifted in frequency to 1450 cm^{-1} in D_2O, consistent with the expectation that the amides would undergo H/D exchange as a result of the slow random coil to β-sheet transition in the absence of salt. The pD of the samples did not change after two weeks for samples incubated at pDs < 6, whereas a 2−3 unit pD decrease was observed for samples with starting pDs of > 7. This is likely a result of the loss of protons to the solution from the positive ammonium charges upon self-assembly due to quaternary structural dependent pK_a perturbations.

Discussion

Studies focused on understanding the mechanism of amyloid fibril formation have been intensely pursued by numerous groups.[9,10,33,62−74] Although amyloid fibrils are similar at the

(63) Colon, W.; Kelly, J. W. *Biochemistry* **1992**, *31*, 8654−8660.
(64) Booth, D. R.; Sunde, M.; Bellotti, V.; Robinson, C. V.; Hutchinson, W. L.; Fraser, P. E.; Hawkins, P. N.; Dobson, C. M.; Radford, S. E.; Blake, C. C. F.; Pepys, M. B. *Nature* **1997**, *385*, 787−793.
(65) Wetzel, R. *Cell* **1996**, *86*, 699−702.
(66) Hurle, M. R.; Helms, L. R.; Li, L.; Chan, W.; Wetzel, R. *Proc. Natl. Acad. Sci. U.S.A.* **1994**, *91*, 5446−5450.
(67) Jarrett, J.; Lansbury, P. T., Jr. *Cell* **1993**, *73*, 1055−1058.

level of their ultimate quaternary structure, the degree of similarity in their assembly pathways remains unclear. That said, striking similarities are observed when the assembly pathways of peptidomimetic **B** are compared with the human amyloid proteins calcitonin and amylin. The major difference being the width of the filament that is formed for calcitonin (40 Å), amylin (50 Å), and peptidomimetic **B** (55 Å).[42,43,75,76] The common themes governing the assembly of peptidomimetic **B** and other amyloidogenic proteins are also evident from electron microscopy, atomic force microscopy and X-ray fibril diffraction studies, suggesting that simple peptides may be suitable model systems for studying amyloid fibril formation and β-sheet mediated self-assembly in general. The data outlined above demonstrate that peptidomimetic **B** self-assembles into polymorphic β-sheet quaternary structures including protofilaments, filaments, fibrils and ribbons that are generally soluble in aqueous solution. The ability to control the distribution of quaternary structures formed by manipulating solution conditions including pH and ionic strength provides insights into the assembly mechanism(s).

Linked Quaternary and Secondary Structural Changes Initiate Assembly. Peptidomimetic **B** undergoes a transition from a random coil to a soluble β-sheet quaternary structure in water (pD 1−12), after 2 weeks or in acetate buffer (pH 3−6) after 4−8 weeks (within 24 h in the presence of NaCl). Analytical ultracentrifugation and microscopy results show that β-sheet secondary structure formation detected by far-UV CD and FT-IR studies coincided in every case with the self-assembly of peptidomimetic **B**, suggesting linked equilibria. The red-shifted far-UV CD minimum (225 ± 3 nm) and maximum (200 nm) are consistent with an associated antiparallel β-sheet structure[78,79] as are the FT-IR bands at 1629 cm^{-1} and 1688 cm^{-1}. The high-intensity CD maximum near 200 nm and the red-shifted minimum near 225 nm ± 3 are consistent with spectra reported earlier and spectra based on theoretical calculations for assembled β-sheet structures.[77,78,79] The high solubility of the very long fibrilar structures in addition to the aromatic contribution of the dibenzofuran skeleton to the far-UV CD spectrum may also contribute to the high ellipticities observed.

Pathway of Assembly of Peptidomimetic B into Protofilaments, Filaments, Fibrils, and Ribbons. On the basis of the electron microscopy, atomic force microscopy, and X-ray fiber diffraction data presented here, we propose that peptidomimetic **B** self-assembles affording quaternary structures with an average width of 25 Å and height of 6 Å, corresponding to the width and height of a single cross-β-sheet monolayer, Figures 8, 14. Face to face dimerization of the cross-β-sheet quaternary structure mediated by hydrophobic interactions yields a 10−12 Å thick bilayer, referred to as protofilament, Figures 8, 9A, and 14 **(a)**. These protofilaments further elongate to about 60 nm and interact via lateral association to form filaments 50−60 Å in width, composed of two protofilaments, Figures 9A, 14 **(b)**. We anticipate that hydrophobic interactions between the templates mediate the formation of filaments (dimerization of protofilaments) and association of filaments into more complex quaternary structures, a hypothesis we have begun to test. The observation of ribbon structures with measured heights of 11, 23, and 31 Å at pH 5.8 (50 μM, 75 mM NaCl, Figure 8B) suggests that face-face stacking of peptidomimetic **B** assemblies continues beyond a single cross-β bilayer structure (11 Å) under some conditions, yielding multilayered fibrils and ribbons.

Flat filaments (50−60 Å in width) can associate to form intermediate ribbon structures where the filaments are loosely associated and lack a defined helical twist, Figures 7B, 14 **(c)**. Alternatively, flat and tightly packed ribbon structures can also form from two or more filaments, Figures 7B, 14 **(e)**. Two- or four-filament ribbons can also form 2 (100−130 Å in diameter) or four-filament twisted fibrils (240−260 Å in diameter) by virtue of the right-handed twist exhibited by each β-strand composing the filaments, Figures 7A, 9, 14 **(d)**. The extent of the twist seems to be quite variable, suggesting that very small differences in free energy are associated with twisting the sheet quaternary structures. Ribbon assemblies composed of less than six 50−60 Å protofilaments were observed to exhibit axial cross over points, whereas ribbons of more than six protofilaments were generally flat and exhibited periodic creasing, Figures 14 **(f)** and 7B. Although such creasing has been observed for calcitonin, we cannot exclude the possibility that it arises from interaction of the ribbons with the hydrophobic Cu coated grid since only flat ribbons are observed on a mica surface by AFM (no tubes, Figure 1E). In addition, time course electron microscopy data provide evidence for a likely morphological interconversion between the fibrils and ribbon assemblies through an intermediate structure such as that shown in Figure 14 **(g)**, suggesting an equilibrium between the two structure exists which is sensitive to solution conditions and incubation time (Figure 9B). The coexistence of many of the quaternary structures discussed above is well documented in the figures within (Figures 7, 8, 9), whereas the relative amount of each species present in the sample is highly dependent on the peptide concentration and solution conditions (pH, ionic strength, buffer counterions). Occasionally, we observed fibrils and ribbons that break revealing the architectures described above, for example, Figures 5B, 7B.

Time dependent studies reveal the disappearance of protofilaments as the population of filaments grows, Figure 9A. The latter decrease in the population as fibrils (Figure 7A) and ribbons (Figure 7B) predominate suggesting that quaternary structures of increasing complexity are formed as a result of the self-association of common building blocks, the protofilaments and/or filaments. In general the observation of all the supramolecular structures was not possible under one set of conditions, hence a summary of the conditions and biophysical methods used to generate and characterize each structure are shown in Table 1.

The presence of intermediates in the assembly pathway of many amyloid proteins has been reported by several groups and is currently emerging as a mechanistic theme in amyloid fibril

(68) Kelly, J. W. *Curr. Opin. Struct. Biol.* **1996**, *6*, 11−17.
(69) Kelly, J. W. *Structure* **1997**, *5*, 595−600.
(70) Selkoe, D. J. *Science* **1997**, *275*, 630−631.
(71) Lansbury, P. T., Jr. *Proc. Natl. Acad. Sci., U.S.A.* **1999**, *96*, 3342−3344.
(72) Patino, M. M.; Liu, J. J.; Glover, J. R.; Lindquist, S. *Science* **1996**, *273*, 622−626.
(73) Lambert, M. P.; Barlow, A. K.; Chromy, B. A.; Edwards, C.; Freed, R.; Liosatos, M.; Morgan, T. E.; Rozovsky, I.; Trommer, B.; Viola, K. L.; Wals, P.; Zhang, C.; Finch, C. E.; Krafft, G. A.; Klein, W. L. *Proc. Nat. Acad. Sci. U.S.A.* **1998**, *95*, 6448−6453.
(74) Lansbury, P. T., Jr.; Costa, P. R.; Griffiths, J. M.; Simon, E. J.; Auger, M.; Halverson, K. J.; Kocisko, D. A.; Hendsch, Z. S.; Ashburn, T. T.; Spencer, R. G. S.; Tidor, B.; Griffin, R. G. *Nat. Struct. Biol.* **1995**, *2*, 990−998.
(75) Goldsbury, C. S.; Cooper, G. J.; Goldie, K. N.; Muller, S. A.; Saafi, E. L.; Gruijters, W. T.; Misur, M. P.; Engel, A.; Aebi, U.; Kistler, J. *J. Struct. Biol.* **1997**, *119*, 17−27.
(76) Glichrist, P. J.; Bradshaw, J. P. *Biochim. Biophys. Acta* **1993**, *1182*, 111−114.
(77) Choo, D. W.; Schneider, J. P.; Graciani, N. R.; Kelly, J. W. *Macromolecules* **1996**, *29*, 355−366.
(78) Kelly, M. M.; Pysh, E. S.; Bonora, G. M.; Toniolo, C. *J. Am. Chem. Soc.* **1977**, *99*, 3264−3266.
(79) Perczel, A. K.; Fasman, G. D. *Proteins: Struct., Funct., Genet.* **1992**, *13*, 57−69.

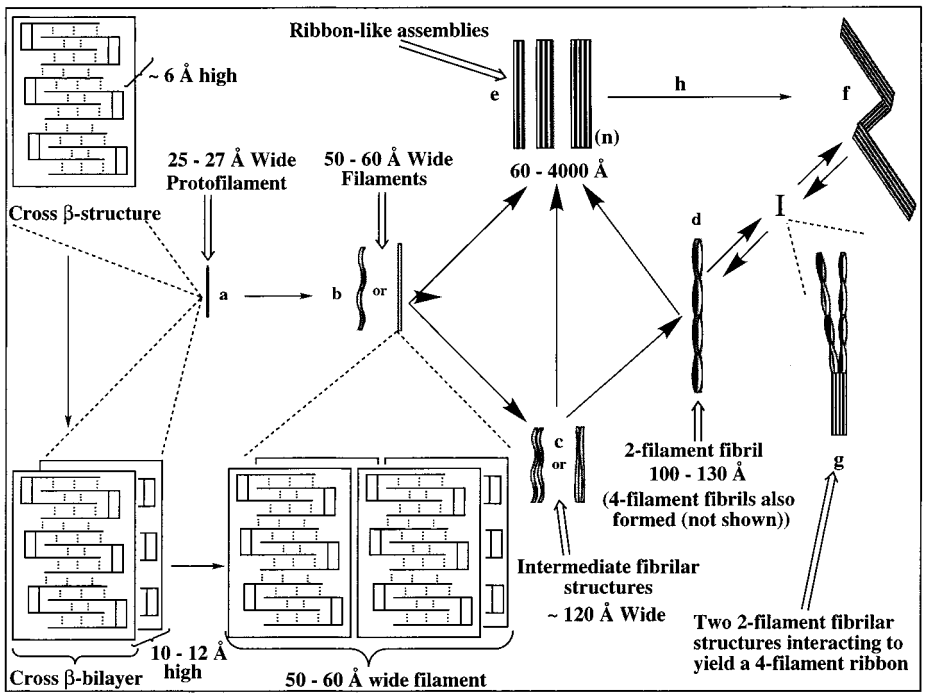

Figure 14. Schematic illustration summarizing the self-assembly pathway envisioned to occur for peptidomimetic **B** that is consistent with the EM, AFM, X-ray fiber diffraction, and time course electron microscopy data over the pH range of 1−12. The apparent route to protofilaments, filaments, fibrils, and ribbons is shown.

Table 1.

entry	pH	buffer[a]	incubation time at 25 °C	secondary structure	dominant morphology observed	architecture diameter (Å)	technique used
1	1−10	D_2O[c]	24 h	random coil	–	–	–
2	1−12	D_2O[c]	2 weeks	β-sheet	2 filament fibrils (pD 1,7−12)	100−130	TEM, Figure 5B
					4 filament fibrils (pD 4−6)	240−260	Figure 14 d
3	4.8	acetate	1−20 h	β-sheet	protofilaments filaments	25−27 60	TEM, Figure 7A
4	4.8	acetate	2 weeks	β-sheet	2 filament helical fibrils	100−130	TEM, Figure 7A
5	5.8	acetate	2 weeks	β-sheet	ribbons composed of 3−36 flat filaments (65 Å)		TEM, Figures 7B, 14c AFM, Figure 8
6	7−10[b]	phosphate or carbonate	4−24 h	β-sheet	heterogeneous array of quaternary structures, including rods.		TEM, Figure 7C

[a] Both acetate and phosphate (50 mM) buffers contained 75 mM NaCl. [b] Carbonate−bicarbonate buffer used for studies at pH 10. [c] D_2O is not buffered.

formation.[20−23,25,28,71,73] The self-assembly of a common core structure into protofilaments, filaments and fibrils suggest that all of these quaternary structures including others that have not yet been detected should be considered as a possible source of pathology in amyloid diseases. Structural evaluation of these species has proven to be a difficult task, mainly due to the difficulty of populating and isolating specific quaternary structures in a highly enriched form. The ability to populate highly enriched quaternary structural types of peptidomimetic **B**, such as two-filament fibrils (Figure 12A) is encouraging. Such stabilization should allow us to characterize the biological properties of these quaternary structural intermediates and thus evaluate their role in neurodegenerative disease. Of keen interest is the fact that peptidomimetic **B** fibrils activate the complement cascade to differing extents depending on the exact morphology of the fibrils in solution. In some cases the extent of activation is similar to that exhibited by Aβ (1−42) and Aβ (27−35) fibrils, which have been demonstrated to be very good activators of the complement cascade, a process thought to be important in amyloid neurotoxicity (data not shown).[83] These results suggest that authentic amyloid proteins may yield a highly enriched population of one quaternary structure under the appropriate conditions. Indeed, we have recently shown that protofilaments of the amyloid protein transthyretin can be generated as the major species at pH 7.5.[21,82]

Basis of pH- and Salt-Dependent β-Sheet-Mediated Self-Assembly. The pH controlled β-sheet-mediated self-assembly of peptidomimetic **B** can be explained by the neutralization of

(80) Barbas, C. F., III; Heine, A.; Zhong, G.; Hoffman, T.; Gramatikova, S.; Bjornestedt, R.; List, B.; Anderson, J.; Stura, E. A.; Wilson, I. A.; Lerner, R. *Science* **1997**, *278*, 2085−2092.
(81) Highbarger, L. A.; Gerlt, J. A.; Kenyon, G. L. *Biochemistry* **1996**, *35*, 41−46.
(82) Lashuel, H. A.; Wurth, C.; Woo, L.; Kelly, J. W. *Biochemistry* **1999**, *38*, 13560- 13573.
(83) Bradt, B. M.; Kolb, W. P.; Cooper, N. R. *J. Exp. Med.* **1998**, *188*, 431−438.

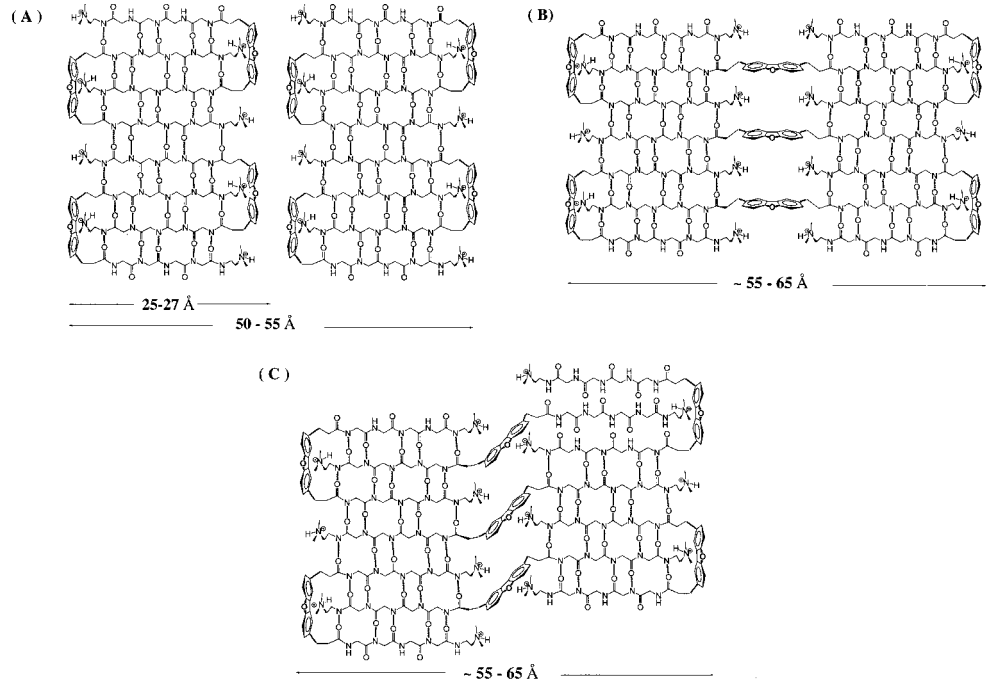

Figure 15. Schematic representation of possible mechanisms of peptidomimetic **B** protofilament assembly yielding filaments. Simple lateral protofilament association mediated by hydrophobic interactions between the dibenzofuran templates is shown (A) An additional component to protofilament association may include strand swapping (B, C).

a fraction of its dmda ammonium groups (Figure 2) in a quaternary structure dependent fashion. The peptidomimetic **B** monomer carries at most two charges, one at the C-termini of each β-strand, having pK_a's in the range of 10−11. Biophysical studies demonstrate that this pK_a does not coincide with the pH dependent quaternary structures exhibited by peptidomimetic **B**, Table 1. The arrangement of β-strands in the peptidomimetic **B** cross-β-sheet depicted in Figure 2B would place the charged ammonium groups in a hydrophobic environment (adjacent to the dibenzofuran skeleton) resulting in a drop in pK_a. Further clustering of ammonium cations is likely to occur during higher order assembly, for example face-to-face assembly to form a bilayer, protofilament association to yield filaments and filament assembly to afford fibrils, Figure 14. This type of association undoubtedly results in successive pK_a decreases such that a significant fraction of the tertiary ammonium groups will be present in the tertiary amine form at pH 7.0. The perturbations of the pK_a resulting from quaternary structure formation (e.g., protofilaments, filaments, ribbons, and fibrils) in combination with the pH and ionic strength of the solution appear to dictate which assemblies can form. The change of pK_a from 10.8 to 7 in a quaternary structure dependent fashion is within the observed range of pK_a shifts reported previously for Lys side chain placed in a hydrophobic environment or in a cationic environment (1−4.5 pK_a units).[77,80,81] The nature of the neutralizing anion seems to be important in controlling the β-sheet quaternary structures afforded as well. For example at constant pH (5.7), the acetate counterion yields highly ordered ribbonlike fibrilar assemblies, whereas the divalent phosphate counterion yields filaments that do not assemble into ordered quaternary structure(s) such as fibrils and ribbons.

Strand Swapping Hypothesis. It is interesting that two protofilaments assemble to form a filament which appear to form fibrils that always seem to have an even number of protofilaments. This observation leads one to speculate that it may be thermodynamically favorable for two protofilaments to undergo an intermolecular strand swap which would explain why protofilaments assemble as pairs and why filaments are so stable. Figure 15 depicts the type of strand swap that we envision. This idea was conceived from the domain swapping arguments introduced into the protein the literature by the Eisenberg laboratory.[33,84−87] The calculated width of two filaments (CPK modeling) linked via a domain swapping mechanism is within the range of 55−65 Å, the exact width depending on the orientation of the dibenzofuran template and the dmda group, Figure 15B and C. This is very similar to the observed width of single filaments of peptidomimetic **B** (∼60 Å). If the interface that mediates protofilament and filament assembly is the same as envisioned, then strand swapping could also occur between interacting filaments by an analogous mechanism. The dibenzofuran template can adopt a low energy conformation which could allow such a strand swap.[88] The proposed domain swapping hypothesis is consistent with the size of the filaments, but we currently have no further experimental data supporting or refuting this possibility.

Extending the Conformational Change Hypothesis to Peptide Quaternary Structure Interconversions. Conformational changes are a requirement for the conversion of folded proteins into amyloid fibrils via alternatively folded states.[21,63,64,68,82,89] In this study it is clear that a transition from a random coil to a β-sheet conformation is linked to quaternary structure formation, as in the case of the peptide Aβ associated with Alzheimer's disease.[74,90] The possibility that conformational

(84) Bennett, M. J.; Choe, S.; Eisenberg, D. *Proc. Natl. Acad. Sci. U.S.A.* **1994**, *91*, 3127−3131.
(85) Bennett, M. J.; Schlunegger, M. P.; Eisenberg, D. *Protein Sci.* **1995**, *4*, 2455−2468.
(86) Liu, Y.; Hart, P. J.; Schlunegger, M. P.; Eisenberg, D. *Proc. Natl. Acad. Sci. U.S.A.* **1998**, *95*, 3437−3442.
(87) Schlunegger, M. P.; Bennett, M. J.; Eisenberg, D. *Adv. Protein Chem.* **1997**, *50*, 61−122.
(88) Tsang, K. Y.; Diaz, H.; Graciani, N.; Kelly, J. W. *J. Am. Chem. Soc.* **1994**, *116*, 3988−4005.
(89) Lai, Z.; Colon, W.; Kelly, J. W. *Biochemistry* **1996**, *35*, 6470−6482.
(90) Kelly, J. W.; Lansbury, P. T., Jr. *Amyloid: Int. J. Exp. Clin. Invest.* **1994**, *1*, 186- 205.

changes take place after partial assembly has been proposed by Teplow and co-workers.[27] The idea is that the β-amyloid monomer, either free in solution or complexed at the end of the protofilament, undergoes further conformational changes that appear to be the rate-determining step of Aβ fibril elongation. Herein, we have shown that protofilaments and fibril assemblies of differing diameters can undergo further conformational changes at various stages in the assembly pathway (e.g., fibril-to-ribbon transitions), resulting in quaternary structural interconversions (Figure 9B). This hypothesis has important implications for explaining the morphological differences observed for amyloid proteins and for the different prion strains, and suggests that a slow equilibrium between different morphologies of the same peptide/protein exist under appropriate conditions. Solution conditions nicely control the assembly pathway presumably by the extent of charge neutralization which controls the rate at which conformational changes and filament assembly occurs at each stage of quaternary structural formation.

Prospects for Designing β-Sheet-Based Materials. The ability of peptidomimetic **B** to self-assemble into polymorphic β-sheet quaternary structures is based on molecular recognition principles. The intermolecular forces can be increased or attenuated to change the distribution of quaternary structures afforded by manipulating the structure of the peptidomimetic or by changing the solution conditions. The dibenzofuran template not only preorganizes the peptidomimetic for dimerization and further assembly, but also provides a hydrophobic edge which seems to promote protofilament and filament assembly via the hydrophobic effect. The importance of the dibenzofuran template in quaternary structure formation is supported by recent findings that a VT repeat of less than 5 (10 residues in total) is unable to undergo intermolecular association.[4] The potential to vary the hydrophobicity of the template, the length of the peptide strands (diameter of protofilament), the nature of side chains and the strand termini by straightforward solid-phase peptide synthesis methods should prove very powerful for the preparation of solid-state materials and for further understanding the mechanism(s) of self-assembly. Furthermore, the important role played by the aqueous buffer components should be equally significant for manipulating the quaternary structures generated.

Experimental Section

General Methods and Materials. Dibenzofuran **(1)** used in these studies was purchased from Lancaster and purified by sublimation at 1 mm vacuum (75 °C) using a water-cooled condenser. Dichloromethane and toluene were distilled from calcium hydride prior to use. Anhydrous dimethylformamide (DMF) and *N*-methylpyrrolidone (NMP) were purchased from Aldrich. Triethylamine (TEA) and diisopropylethylamine (DIEA) were refluxed over ninhydrin, distilled, and redistilled again from calcium hydride to obtain the pure, anhydrous TEA. Ethyl acrylate (Kodak and Aldrich), pentafluorophenol (PCR Fluoroorganics), trifluoroacetic acid (TFA, Solvay), and other reagents were used without further purification. Melting points were obtained on a Fisher-Johns apparatus and are uncorrected. Routine NMR spectra were obtained on a Varian XL-200E. Semi-preparative HPLC was carried out on either a dual pump system equipped with Altex 110A pumps and an Altex 420 computerized controller or a Waters model 600E LC system. The column used was a Waters RCM Delta Pak C_{18} (15m, 300A, 25 × 100 mm), and the peptides were detected with a Knauer 86 variable wavelength UV detector. Solvent A was 95% water, 5% acetonitrile, and solvent B was 95% acetonitrile, 5% water; both were acidified with 0.2% TFA.

2,8-Diiododibenzofuran (2).[46] To a 500 mL round-bottomed flask, equipped with a reflux condenser was added dibenzofuran (16.8 g, 0.1 mol), iodine (19.7 g, 0.08 mol) and iodic acid (7.7 g, 0.044 mole). To the solids were added 200 mL of glacial acetic acid, 15 mL of water, 2 mL of sulfuric acid, and 10 mL of carbon tetrachloride. The mixture was thermostatically heated to 65 °C in an oil bath and stirred for 24 h. Product precipitated throughout the reaction and the color of the solution changed from purple (iodine) to light brown. After the heterogeneous mixture was allowed to cool to room temperature, the solid was filtered out and washed with acetic acid (30 mL). The product was dried under vacuum to yield 35.4 g of the crude 2,8-diiododibenzofuran (82%) as a pink-brown powder. ^{1}H NMR analysis confirmed the crude product with no detectable monosubstituted product or starting material. ^{1}H NMR ($CDCl_3$) δ 8.18 (d, J = 1.9 Hz, 0.5 Hz, 2H), 7.72 (dd, J = 8.6 Hz, 1.9 Hz, 2H), 7.31 (dd, J = 8.9 Hz, 0.5 Hz, 2H). ^{13}C NMR ($CDCl_3$) δ 155.6, 136.4, 129.7, 125.4, 113.8, 86.1. The product was recrystallized from benzene:methanol (60% yield, mp 178 °C). ESIMS *m*/*z* for $C_{12}H_6I_2O$ [M^+] calcd 419.8508, obsvd 419.8539.

2,8-Dibenzofuranbis(ethyl-3-propenoate) (3). To an oven dried 100 mL round-bottomed flask with a magnetic stir bar cooled under N_2 was added 2,8-diiododibenzofuran (10.5 g, 25 mmol) and palladium acetate (0.112 g, 0.5 mmol). The flask was flushed with dry nitrogen and charged with ethyl acrylate (6.8 mL, 62.5 mmol). An oven dried condenser was attached to the flask and cooled under N_2, after which triethylamine (8.7 mL, 62.5 mmol) and anhydrous *N*,*N*′-dimethylformamide (30 mL) were added down the condenser. The mixture was heated with stirring in an oil bath at 98 °C for 2.5 h. The reaction was then allowed to cool, dissolved in 200 mL of methylene chloride, poured into a 500 mL separatory funnel, and washed with 250 mL of water five times. The dichloromethane layer was dried over sodium sulfate (anhydrous), and the organic solvent was removed under reduced pressure. The resulting gray solids were dried under vacuum to afford 9.07 g of crude product (99%). ^{1}H NMR ($CDCl_3$) δ 8.09 (d, J = 1.8 Hz, 2H), 7.83 (d, J = 15.9 Hz, 2H), 7.66 (dd, J = 8.6 Hz, 1.8 Hz, 2H), 7.55 (d, J = 8.7 Hz, 2H), 6.49 (d, J = 16 Hz, 2H), 4.29 (q, J = 7 Hz, 4H), 1.36 (t, J = 7.1 Hz, 6H). ^{13}C NMR ($CDCl_3$) δ 167.0, 157.7, 144.2, 129.9, 127.7, 124.3, 120.6, 117.7, 112.3, 60.5, 14.4. Analytical samples were recrystallized from acetone or DMF; mp 157−159 °C. EIMS *m*/*z* for $C_{22}H_{20}O_5$ [M^+] calcd 364.1311, obsd 364.1303.

2,8-Dibenzofuranbis(3-propionic Acid) (4). In a 250 mL round-bottomed flask fitted with a reflux condenser, crude 2,8-bis(ethyl 3-propenoate)dibenzofuran (9.1 g, 25 mmol) and NaOH (8.0 g, 0.2 mol) were heated to 85 °C in 180 mL of absolute ethanol. After 2.5 h of stirring at reflux, the milky reaction was cooled to room temperature and further cooled in an ice bath. The solid product was filtered out and dried under vacuum to afford crude 2,8-dibenzofuran-bis(sodium 3-propenoate).The crude product was then dissolved in 250 mL of distilled water in a 500 mL parr bottle with sonication. To the solution was added 10% Pd/C (1.0 g) and the bottle connected to a hydrogenation apparatus. The solution was degassed by aspiration and flushed with hydrogen. This degassing/flush procedure was repeated three times, and the bottle was finally charged with hydrogen to 45 psi. The reaction was allowed to proceed until complete as judged by ^{1}H NMR. After the hydrogen uptake was complete, the catalyst was filtered out using a 0.22 μm pore size acetate filter. The auburn-colored liquid was cooled in an ice bath, and concentrated HCl was added dropwise with mixing to acidify the solution to pH 1. The solids were filtered out and dried under vacuum to afford 7.14 g (95%) of crude 2,8-dibenzofuranbis-(propionic acid) as a white powder; mp 209−213 °C . The product was recrystallized from ethanol/water; mp 219−221 °C . ^{1}H NMR (DMSO-d_6) δ 12.1 (2H, s), 7.93 (d, J = 2 Hz, 0.5 Hz, 2H), 7.51 (d, J = 8.5 Hz, 2H), 7.35 (dd, J = 8.5 Hz, 1.6 Hz, 2H), 2.98 (t, J = 7.4 Hz, 4H), 2.52 (t, J = 7.4 Hz, 4H). ^{13}C NMR (DMSO-d_6) δ 174.0, 154.7, 136.0, 128.1, 123.8, 120.6, 111.6, 36.0, 30.6. ESIMS *m*/*z* for $C_{18}H_{16}O_5$ [M^+] calcd 312.0998, obsd 312.0994.

2,8-Dibenzofuranbis(pentafluorophenyl-3-propionate) (5). To an oven dried 25 mL round-bottomed flask cooled under N_2 were added 2,8-dibenzofuranbis(3-propionic acid) (1.57 g, 5 mmol) and pentafluorophenol (1.92 g, 10.2 mmol). The flask was flushed with dry nitrogen, and the solids were dissolved in ethyl acetate/DMF (8:3, 14 mL). The solution was cooled to 0 °C using an ice bath, and *N*,*N*′-dicyclohexylcarbodiimide (2.27 g, 11.1 mmol) was added. After 1 h of cooling, the reaction was allowed to warm to room temperature and stirred for an additional 2.5 h. The reaction products were then filtered, and the

solid was washed with 10 mL of ethyl acetate; the solvent was then removed under reduced pressure. The resulting solid was redissolved in 20 mL of ethyl acetate and cooled in an ice bath for 1 h. The residual urea was filtered out from the soluble product and the solvent removed under reduced pressure to afford the crude product. The product was recrystallized from hexane to yield 1.99 g (62%) of 2,8-dibenzofuranbis-(pentafluorophenyl-3-propionate) as white needles; mp 167−168 °C . ^{1}H NMR ($CDCl_3$) δ 7.82 (d, J = 1.4 Hz, 2H), 7.52 (d, J = 8.3 Hz, 2H), 7.36 (d, J = 8.4 Hz, 1.7 Hz, 2H), 3.26 (dt, J = 7 Hz, 1.5 Hz, 4H), 3.07 (dt, J = 1.5 Hz, 7 Hz, 4H). ^{13}C NMR ($CDCl_3$) δ 168.7, 155.5, 133.9, 127.5, 124.4, 120.1, 111.8, 35.6, 30.6. FT-IR (KBr) cm^{-1} 1784 (ester), 1520 (C−F), 992 (C−F). EIMS *m/z* for $C_{30}H_{14}F_{10}O_5$ [M^+] calcd 644.0682, obsd 644.0672.

Synthesis of Protected Peptide Fragments. Manual solid-phase peptide synthesis was carried out using oxime resin synthesized in our laboratory having a loading of approximately 0.6 meq/g.[91,92] Dichloromethane (DCM), isopropyl alcohol (IPA), and dimethylformamide (DMF) used were reagent grade. DMF was stored over 4 Å molecular sieves to reduce the amount of primary and secondary amines present in the solvent. Side-chain-protected Boc-amino acids were purchased from Advanced Chemtech. The TFA-deprotecting solution (TFA:DCM: thioanisole (35:64:1)) was stored under dry nitrogen and protected from light. DIEA was prepared as described earlier. All oxime resin reactions were carried out using 10 mL of solvent per gram of resin.

The resin was prepared for attachment of the first Nα-*t*-Boc-protected amino acid by washing the resin in a synthesis vessel with DCM (1 × 1 min), IPA (1 × 1 min) and DCM (2 × 1 min). The first amino acid was loaded onto the resin by shaking 1.6 equiv of diisopropylcarbodiimide activated Nα-*t*-Boc amino acid with oxime resin for 24 h in DCM. The resin was then washed with DCM (2 × 1 min), IPA (2 × 1 min), DCM (1 × 1 min), IPA (1 × 1 min), and DCM (3 × 1 min). All remaining free oxime groups were then capped by shaking the resin with trimethylacetic anhydride (3 mmol/g of resin) in DCM for 24 h followed by washes with DCM (2 × 1 min), IPA (2 × 1 min), DCM (1 × 1 min), IPA (1 × 1 min), and DCM (3 × 1 min). The following cycle was used for the coupling of each amino acid: TFA prewash (35% TFA x 1 min), TFA deprotection (35% TFA × 30 min), DCM (2 × 1 min), IPA (2 × 1 min), DCM (1 × 1 min), IPA (1 × 1 min), DCM (3 × 1 min), coupling of preactivated Nα-*t*-Boc amino acid (1 × 3 h), DCM (2 × 1 min), IPA (2 × 1 min), DCM (1 × 1 min), IPA (1 × 1 min), DCM (3 × 1 min). Each coupling step and deprotection step was monitored by the Kaiser ninhydrin test. Upon completion of a peptide sequence, the resin was dried under vacuum.

All Nα-*t*-Boc amino acids were preactivated as described: Nα-*t*-Boc amino acid (3 equiv) and BOP reagent (2.9 equiv) were dissolved (or partially dissolved) in DCM (7−8 mL) and cooled to 4 °C . The cooled reagents were then activated with DIEA (6 equiv), and DMF (1 mL) was added. The amino acid was allowed to preactivate for 10−15 min at room temperature after which it was added to the trifluoroacetate ammonium form of the resin, and DCM was added to bring the volume up to 10 mL or to such a point that the resin flows evenly. For the third amino acid added to the resin 6 equiv of Nα-*t*-Boc amino acid, 5.9 equiv of BOP reagent, and 9 equiv of DIEA were utilized to impede the formation of diketopiperazine by intramolecular cyclization of the first two amino acids.

Nucleophilic Cleavage of Peptides from the Oxime Resin. To a 20 mL of peptide synthesis vessel was added oxime-Thr(bzl)-Val-Thr-(bzl)-Val-Boc resin (0.8 g). The resin was swollen in DCM and *N,N*-dimethylethylenediamine (dmda, 1.4 mL, 12.8 mmol, 20 equiv) was added, and the contents were agitated for 4 h. The resulting solution was drained into a sidearm filtration flask (125 mL) and the resin washed with DCM (2 × 10 mL), 1:1 DCM/DMF (1 × 10 mL), and DCM (1 × 10 mL), collecting all of the washes. The combined washes were concentrated under reduced pressure to ∼5−10 mL, and the solution of crude peptide was added dropwise with stirring to distilled water (150 mL). The precipitated peptide was filtered out and dried to afford 235 mg of product. Deprotection of the Boc group from the N terminus of the peptide was accomplished using 1:3 TFA:DCM (10 mL, without thioanisole) for 1 h. The solution was concentrated to an oil under reduced pressure, redissolved in 40% acetonitrile in water, filtered, and the acetonitrile was removed under reduced pressure. The sample was frozen and lyophilized to afford 185 mg (89%) of Val-Thr(bzl)-Val-Thr(bzl)-dmda·2TFA **(6)** which was >90% pure as ascertained by C_{18} RP-HPLC (230 nm). The peptide was purified by C_{18} RP-HPLC, the acetonitrile was removed under reduced pressure, and the peptide was isolated by lyophilization.

Solution-Phase Peptide Coupling. To an oven dried, 50 mL round-bottomed flask was added Val-Thr(bzl)-Val-Thr(bzl)-dmda·2 Tfa (196 mg, 0.219 mmol) and 2,8-dibenzofuranbis(pentafluorophenyl-3-propionate) (**5**)(50 mg, 0.078 mmol). The solids were dissolved in anhydrous DMF (20 mL) with stirring and a 10 μL aliquot was analyzed by C_{18} RP-HPLC. The reaction was initiated by the addition of DIEA (81 μL, 0.45 mmol) to neutralize the amino terminus of the peptide (monitored using hydrated pH paper). The reaction was monitored by HPLC to determine the endpoint of the reaction; approximate reaction time was 4 h. Once the reaction was complete, the peptide was precipitated by diluting the reaction in 200 mL of water. The peptide was isolated by filtration (0.22 μm nylon membrane) and dried in vacuo, affording 95 mg of crude Diac(Val-Thr(bzl)-Val-Thr(bzl)-dmda)2 **(7)** (Diac = dibenzofuran diacid). The identity of the product was ascertained by MALDI-TOF-MS.

Solution-Phase Peptide Deprotection. To a 25 mL round-bottomed flask was added Diac(Val-Thr(bzl)-Val-Thr(bzl)-dmda)$_2$ (180 mg, 102 mmol) which was dissolved in methanol (2 mL) and a minimum amount of formic acid (approximately 3 mL). The flask was flushed with N_2, and 10% Pd/C (102 mg) was added. The nitrogen atmosphere was then replaced with an atmosphere of hydrogen gas. The flask was purged with hydrogen, and the reaction was carried out under one atmosphere of hydrogen gas. The reaction was monitored by C_{18} RP-HPLC, examining the chromatogram for the emergence of the deprotected peptide. After 4−5 h the Pd/C was filtered, and the methanol was removed under reduced pressure and the thick, heterogeneous solution was diluted with water (10 mL). The pH of the solution was adjusted to approximately 7 and the catalyst filtered out using a 0.22 μm acetate membrane. The solution was analyzed by C_{18} RP-HPLC followed by purification using semipreparative C_{18} RP-HPLC. The acetonitrile in the solution was removed under reduced pressure, and the sample was lyophilized to afford 58 mg (75%) of the deprotected host peptide Diac-(Val-Thr-Val-Thr-dmda)2 **(8)**; ESI/MS ($M + H_{calcd}$ = 1253.5, $M + H_{obsd}$ 1254.0 g/mol).

Analytical Ultracentrifugation. Sedimentation equilibrium runs were performed on peptidomimetic **B** (50 μM) samples (150 μL) at the desired pH, buffer condition and temperature at a rotor speed of 50,000 rpm using a double sector cell with charcoal-filled Epon centerpieces and sapphire windows. All scans were performed at 288 or 256 nm with a step size of 0.001 cm and 25 averaged scans. Samples were allowed to equilibrate for 24 h, and duplicate scans 3 h apart were overlaid to determine that equilibrium had been reached. The data were analyzed by a nonlinear least-squares analysis using the Origin software provided by Beckman. The data were initially fit to a single ideal species model using the following equation to determine the best fitting molecular weight:

$$A_r = \exp[\ \ln(A_0) + (M\omega^2(1 - \bar{v}\rho)/2RT)(x^2 - x_0^2)] + E \qquad \text{(I)}$$

where A_r is the absorbance at radius x, A_0 is the absorbance at a reference radius x_0 (usually the meniscus), $\bar{v}$ is the partial specific volume of peptidomimetic B (0.778 mL/g), ρ is the density of the solvent (g/mL), ω is the angular velocity of the rotor (radian/sec), E is the baseline error correction factor, M is the molecular weight, R is the universal gas constant (8.314×10^7 erg/mole), and T is the temperature (Kelvin).

Sedimentation Velocity. Sedimentation velocity experiments were carried out using 400−420 μL of peptide solution and data were recorded at rotor speeds of 3000−20 000 rpm in continuous mode at 25 °C with a step size of 0.005 cm. The sedimentation velocity absorbance profiles were then analyzed via van Holde and Weischet global boundary analysis to obtain a sedimentation coefficient distribution for all the quaternary structures in solution as described previously.[21] To determine the amount of unsedimented peptide (monomer)

(91) Findeis, M. A.; Kaiser, E. T. *J. Org. Chem.* **1989**, *54*, 3478−3482.
(92) Scarr, R. B.; Findeis, M. A. *Pept. Res.* **1990**, *3*, 238−241.

two radial scans were collected at 3000 rpm (no sedimentation is observed) and 20 000−30 000 rpm (monomer does not sediment), and the percent of monomeric species was calculated using eq II.

$$\%\ \text{of unsedimented peptidomimetic } \mathbf{B} = 1 - (\text{Absorbance}_{(290\ \text{nm},\ 3000\ \text{rpm})} - \text{Absorbance}_{(290\ \text{nm},\ 20{,}000-30{,}000\ \text{rpm})}) \times 100 \quad \text{(II)}$$

Sedimentation equilibrium studies of the unsedimented species were carried out to determine whether a monomer, dimer or a mixture was present in solution.

Far-UV Circular Dichroism. CD spectra were recorded on an Aviv model SF202 spectrometer at 25 °C using a bandwidth of 0.5 nm, a time constant of 100 ms, step size of 0.5 nm, and an averaging time of 1 s. Far-UV CD spectra of peptidomimetic **B** solutions (50 μM) in one of the following buffers were recorded after 24 h of incubation at 25 °C: 50 mM of acetate buffer (at pH 3.4, 4.8, and 5.7), 50 mM phosphate buffer (at pH 5.7, and 7, 8), and 50 mM carbonate−bicarbonate buffer (at pH 10). Samples were prepared from stock solutions (0.5−1 mM) in water and diluted to the appropriate concentration in the desired buffered solution. For the salt-dependence studies the appropriate amount of NaCl was added to each buffer solution before the final pH of the buffer was measured. The concentration of the peptide sample was determined by UV spectroscopy using the extension coefficient of dibenzofuran ($\epsilon_{289} = 17\,780$). The far-UV CD spectra were recorded from 195 to 250 nm using 0.1 cm quartz cells. All spectra were corrected for buffer contribution and reported in units of mean residue ellipticity.[93]

FT-IR Measurements. The lyophilized peptide was dissolved in D_2O, and samples were prepared by dilution of a peptide stock in D_2O solutions which were subsequently adjusted to the desired pD using DCl and NaOD solutions. The solutions were incubated for a week at 25 °C to allow for the slow conversion to β-sheet and then applied to CaF_2 plate. The solvent was evaporated under vacuum. FT-IR spectroscopy was performed on ATI-Mattson Galaxy series 5000 FT-IR spectrometer equipped with an MCT detector. The spectra were recorded at 2 cm^{-1} resolution and represent an average of 232 scans at 25 °C.

Electron Microscopy. The samples were prepared by placing 5 μL of the sample on a glow-discharged carbon-coated grid and allowing the solution to stand for 2 min before removing excess solution. The grid was then washed once with distilled water and once with 1% uranyl acetate before staining the sample with fresh 1% uranyl acetate for another 2 min. The samples were then studied in a Phillips CM-100 electron microscope. The grids were thoroughly examined to get an overall statistical evaluation of the structures present in the sample. All electron micrographs were taken at 100 kV.

Atomic Force Microscopy (AFM). The AFM images were recorded by placing 3−5 μL of the peptide in acetate buffer (50 mM, 75 mM NaCl, pH 4.8 and 5.75) on freshly cleaved mica. After 30 s the mica was gently rinsed twice with 50 μL of 0.2 μm-filtered water to remove salt and loosely bound peptide. The AFM images were collected at ambient temperature on a Nanoscope IIIa multimode scanning probe workstation (Digital Instruments, Santa Barbara, CA) operating in a tapping mode using etched silicon NanoProbes (Probe model TESP, Digital Instruments). The drive frequency was around 250−300 kHz. Scanning speed was at a line frequency of 1.2−2.2 Hz.

X-ray Fiber Diffraction. The peptide was dissolved in filtered (0.22 μm Millipore) distilled water at a concentration of 20 mg/mL and incubated at room temperature for 48 h. A droplet of the solution was placed between two wax plugged glass capillary tubes on a stretch frame and allowed to dry to form a bundle of partially aligned fibers. The specimen was placed on a goniometer head, and X-ray data was collected on a MAR Research image plate (300 mm diameter) using a Cu Kα Rigaku rotating anode X-ray source. Exposure time was 30 min with a specimen-to-film distance of 148.21 mm (2 Å edge plate). Images were examined using Mosflm (A leslie, MRC Cambridge).

Congo Red and Thioflavin Binding Studies. A Congo red stock solution was prepared by dissolving recrystallized Congo red as described previously.[89] The concentration of the Congo red stock was determined by measuring the absorbance of a diluted aliquot at 477 nm ($\epsilon_{477\ \text{nm}} = 34\,722\ cm^{-1}\ M^{-1}$).[94] Buffered Congo red solutions at 2.5 μm were prepared by dilution of an aliquot of the stock solution in 50 mM acetate, phosphate, or carbonate−bicarbonate buffer solutions at the desired pH. Binding studies were carried out by diluting 50 μL of a 50 μM peptide solution to 500 μL of Congo red buffered solution. The resulting solutions were then vortexed and the UV−vis spectra (300−700 nm) was collected immediately. Incubation of the sample did not appear to change the UV absorbance spectra.

Thioflavin T was purchased from Aldrich (70% purity) and was recrystallized from benzene/ethanol (1:1) to afford yellow crystals.[95] Thioflavin T binding assays were performed by addition of 100 μL of 50 μM peptidomimetic **B** solution that had been aged for 3 months to 900 μL solution of 10 μM thioflavin T in phosphate buffer (10 mM phosphate, 100 mM KCl). The solutions were mixed, and fluorescence measurements were recorded in an ATF 105 model Aviv spectrofluorimeter at 25 °C using a 1 cm path length quartz cell. An excitation slit width of 4 nm and an emission slit width of 6 nm were employed. The excitation wavelength was set to 450 nm and emission monitored from 460 to 630 nm.

Acknowledgment. The authors gratefully acknowledge financial support from the National Institute of Health grants R01 GM51105 and R01 DK46335, The Skaggs Institute of Chemical Biology, the Lita Annenberg Hazen Foundation and The American Chemical Society Organic Division predoctoral fellowship to H.A.L. We are grateful to Dr. Peter Lansbury and Dr. James Harper for essential AFM assistance and Dr. Edward Koepf and Dr. Prakash Raman for proofreading the manuscript.

Supporting Information Available: Sedimentaion equilibrium analysis of peptidomimetic **B** (50 μM), Thioflavin T and Congo Red fibril binding data, as well as far-UV CD data after subjecting a pH 7 sample of peptidomimetic **B** in phosphate buffer to sedimentation (PDF). This material is available free of charge via the Internet at http://pubs.acs.org.

JA9937831

(93) Schmid, F. X.; Creighton, T. E., Eds.; *Protein Structure*; *A Practical Approach*; IRL Press: New York, 1989; pp 251−285.

(94) Klunk, W. E.; Pettegrew, J. W.; Abraham, D. J. *J. Histochem. Cytochem.* **1989**, *37*, 1273−81.

(95) LeVine, H. I. *Protein Sci.* **1993**, *2*, 404−410.